Function of the *Drosophila* adhesion-GPCR Latrophilin/CIRL
in nociception and neuropathy

Funktionelle Rolle des *Drosophila* aGPCR Latrophilin/CIRL
in Nozizeption und Neuropathie

Doctoral thesis for a doctoral degree
at the Graduate School of Life Sciences,
Julius-Maximilians-Universität Würzburg,
Section Neuroscience

submitted by

Sven Dannhäuser

from

Fürth, Bayern

Würzburg 2019

Members of the Thesis Committee:

Prof. Dr. Robert J. Kittel

Prof. Dr. Dr. Tobias Langenhan

Prof. Dr. Georg Nagel

Chairman: Prof. Dr. Michael Sendtner

Submitted on: 11th December 2019

Date of Public Defense: 9th March 2020

Acknowledgements

Function of the *Drosophila* adhesion-GPCR Latrophilin/CIRL in nociception and neuropathy

Table of Contents

I. Summary

Touch sensation is the ability to perceive mechanical cues which is required for essential behaviors. These encompass the avoidance of tissue damage, environmental perception, and social interaction but also proprioception and hearing. Therefore research on receptors that convert mechanical stimuli into electrical signals in sensory neurons remains a topical research focus. However, the underlying molecular mechanisms for mechano-metabotropic signal transduction are largely unknown, despite the vital role of mechanosensation in all corners of physiology.

Being a large family with over 30 mammalian members, adhesion-type G protein-coupled receptors (aGPCRs) operate in a vast range of physiological processes. Correspondingly, diverse human diseases, such as developmental disorders, defects of the nervous system, allergies and cancer are associated with these receptor family. Several aGPCRs have recently been linked to mechanosensitive functions suggesting, that processing of mechanical stimuli may be a common feature of this receptor family – not only in classical mechanosensory structures.

This project employed *Drosophila melanogaster* as the candidate to analyze the aGPCR Latrophilin/dCIRL function in mechanical nociception *in vivo*. To this end, we focused on larval sensory neurons and investigated molecular mechanisms of dCIRL activity using noxious mechanical stimuli in combination with optogenetic tools to manipulate second messenger pathways. In addition, we made use of a neuropathy model to test for an involvement of aGPCR signaling in the malfunctioning peripheral nervous system. To do so, this study investigated and characterized nocifensive behavior in *dCirl* null mutants (*dCirlKO*) and employed genetically targeted RNA-interference (RNAi) to cell-specifically manipulate nociceptive function.

The results revealed that *dCirl* is transcribed in type II class IV peripheral sensory neurons – a cell type that is structurally similar to mammalian nociceptors and detects different nociceptive sensory modalities. Furthermore, *dCirlKO* larvae showed increased nocifensive behavior which can be rescued in cell specific reexpression experiments. Expression of bPAC (bacterial photoactivatable adenylate cyclase) in these nociceptive neurons enabled us to investigate an intracellular signaling cascade of dCIRL function provoked by light-induced elevation of cAMP. Here, the findings demonstrated that

dCIRL operates as a down-regulator of nocifensive behavior by modulating nociceptive neurons. Given the clinical relevance of this results, dCirl function was tested in a chemically induced neuropathy model where it was shown that cell specific overexpression of dCirl rescued nocifensive behavior but not nociceptor morphology.

II. Zusammenfassung

Der Tastsinn ist die Fähigkeit, mechanische Reize wahrzunehmen, die für essentielle Verhaltensweisen notwendig sind. Dazu gehören die Vermeidung von Gewebsschädigungen, die Wahrnehmung der Umwelt und soziale Interaktion, aber auch die Propriozeption und das Hören. Daher bleibt die Forschung an Rezeptoren, die mechanische Reize in sensorischen Neuronen in elektrische Signale umwandeln, ein aktueller Forschungsschwerpunk. Die zugrundeliegenden molekularen Mechanismen für die mechanometabotrope Signalübertragung sind trotz der wesentlichen Rolle des Tastsinns in allen Bereichen der Physiologie weitgehend unbekannt.

Adhäsions G-Protein gekoppelte Rezeptoren (aGPCRs), eine große Molekülfamilie mit über 30 Vertretern im Menschen, sind an einer Vielzahl von physiologischen Prozessen beteiligt. Demzufolge wird ein Zusammenhang zwischen diesen Rezeptoren und verschiedenen Erkrankungen des Menschen, wie z. B. Entwicklungsstörungen, Defekte des Nervensystems, Allergien und Krebs, angenommen. Mehrere aGPCRs wurden kürzlich mit mechanosensitiven Funktionen in Verbindung gebracht, was darauf hindeutet, dass die Verarbeitung mechanischer Reize ein gemeinsames Merkmal dieser Rezeptorfamilie ist – nicht nur in klassischen mechanosensorischen Strukturen.

In diesem Projekt wurde *Drosophila melanogaster* verwendet, um die Funktion des aGPCR-Latrophilin/dCIRL in der mechanischen Nozizeption *in vivo* zu analysieren. Zu diesem Zweck konzentriert sich diese Arbeit auf mechano-sensorische Neurone (Typ II Klasse IV) der Fruchtfliegenlarve, um die molekularen Mechanismen der dCIRL-Aktivität zu untersuchen. Hierzu wurden noxische mechanische Reize in Kombination mit optogenetischen Werkzeugen, zur Manipulation der Second-Messenger-Signalübertragung, herangezogen.

Zusätzlich wurde ein Neuropathie-Modell etabliert, um eine Beteiligung des aGPCRs dCIRL am beeinträchtigten peripheren Nervensystem zu testen. Zu diesem Zweck untersucht und charakterisiert diese Studie das nozizeptive Verhalten in dCirl-Nullmutanten *(dCirlKO)* und die RNA-Interferenz (RNAi) Methode, um zellspezifische Manipulationen auszuführen.

Die Ergebnisse zeigen, dass dCirl in spezifischen peripheren sensorischen Neuronen (C4da) transkribiert wird - ein Zelltyp, der Nozizeptoren in Säugern strukturell ähnlich ist und verschiedene nozizeptive sensorische Modalitäten vermittelt.

Darüber hinaus zeigen *dCirlKO*-Larven ein erhöhtes nozizeptives Verhalten, welches mittels zellspezifischer Reexpression gerettet werden kann. Die Expression von bPAC (bakterielle photoaktivierbare Adenylatcyclase) in diesen nozizeptiven Neuronen ermöglichte es, intrazelluläre Signalkaskaden von CIRL zu untersuchen, welche durch lichtinduzierte Erhöhung von cAMP angeregt werden. Dieser Versuch zeigt, dass dCIRL durch die Modulation nozizeptiver Neuronen eine Herabregulation des nozizeptiven Verhaltens bewirkt.

Angesichts der klinischen Relevanz dieses Ergebnisses wurde die dCirl-Funktion in einem chemisch induzierten Neuropathie-Modell getestet. Dabei stellte sich heraus, dass zellspezifische Überexpression von *dCirl* eine ausgeprägte Hyperalgesie reduziert, morphologische Schädigungen hingegen nicht gerettet werden konnten.

1 Introduction

1.1 Nociception

Essential for any scientific work about physiological basis in this field is a clear understanding and definition of nociception and related terms. What exactly is nociception? And how is it different from pain?

In the 1900s, Charles S. Sherrington provided the definition of "nociception" that is the detection of noxious stimuli by nociceptors. Nociception thus is the cognition generated by processing - in the peripheral and central nervous system - of information about the internal or external environment, as generated by the activation of nociceptors (Sherrington, 1906). In this fundamental work, Sherrington additionally described nociceptors, which can be found in the skin, muscles, joints, and viscera and are activated through noxious stimuli such as tissue damage (Sherrington, 1906).

Strictly separated from nociception is the term "pain". The International Association for the Study of Pain (IASP) defines pain in humans as "an unpleasant sensory and emotional experience associated with actual or potential tissue damage" [IASP 1979; (Loeser et al., 2008)]. Pain typically involves a noxious stimulus or event that activates nociceptors but is a product of higher brain center processing – feelings and experiences are involved – whereas nociception can occur in the absence of pain (National Research Council, 2009).

1.1.1 Nociception in mammals

Percipience of nociception provides animals with the opportunity to detect and escape potential harmful stimuli that could detrimentally affect survival. In higher organisms, information received by nociceptors are integrated and processed in the central nervous system (CNS) where pain is then experienced (Schmidt, 2011; Herr et al., 2017). According to the hypothesis published by Sherrington, nociceptors have characteristic thresholds and sensitivities that separate them from other sensory nerve fibers (Sherrington, 1906). Thus different types of noxious stimuli require different types of nociceptors therewith different primary afferent axons can be distinguished. These fibers can be categorized into three main groups, based on anatomical and functional features (Figure 1) (Lumpkin et al., 2010). Most, but not all Aβ-fibers detect non-noxious

mechanical stimuli applied to the skin, muscles and joints. Aδ-fibers are represented by two different classes, that both respond to noxious mechanical stimuli respectively but differ in responsiveness to heat and tissue injury. Polymodal, unmyelinated free nerve ended C-fibers respond to noxious heat as well as to chemical stimuli (e.g. acid, lye or capsaicin) (Schmidt, 2011; Stahl, 2013; Herr et al., 2017).
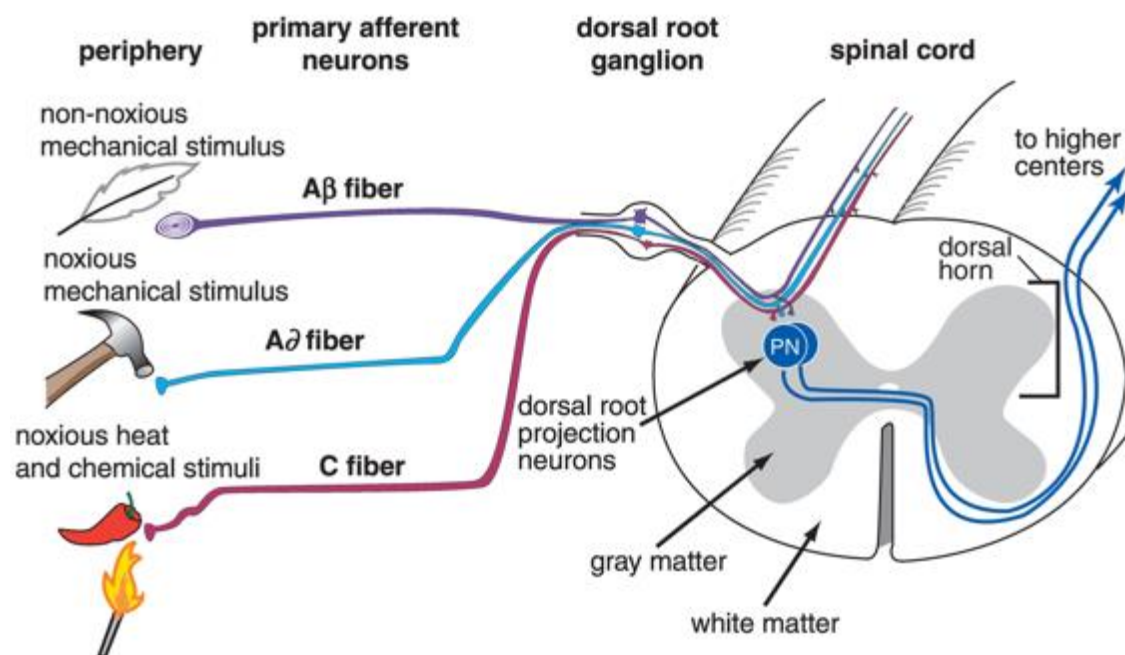
Figure 1. Activation of nociceptive nerve fibers. Aβ-fibers respond to non-noxious mechanical stimuli, Aδ-fibers respond to noxious mechanical stimuli and C-fibers respond polymodal to noxious heat, chemical as well as mechanical stimuli. The Cell bodies of primary afferents are in the dorsal root ganglion (DRG) and their terminals can be found in the spinal cord. They synapse on different dorsal horn projection neuron classes, which project to higher centers through different tracts [taken from (Stahl, 2013)].

Molecular analysis of mechanosensation and the evidence of molecules that constitute the mechanotransduction machinery are limited. Various mechanically gated ion channels have been identified as important key players for mechanosensory transduction in mammals in the recent past. Different predicted ion channel candidates belong into the degenerin/epithelial Na+ channel (DEG/ENaC) and transient receptor potential (TRP) families, which are highly conserved in vertebrates as well as invertebrates (Bazopoulou et al., 2007; Lumpkin et al., 2010; Islam, 2011).

The TRP family is divided into seven subfamilies: TRPC (canonical), TRPV (vanilloid), TRPM (melastatin), TRPP (polycystin), TRPML (mucolipin), TRPA (ankyrin) and TRPN (NOMPC-like). Recently, transient receptor potential ankyrin 1 (TRPA1) channels were identified as important molecules in nociceptive physiology and were proven to be

responsible for sensing noxious heat in vertebrates and invertebrates (Ferrandiz-Huertas et al., 2014; Honjo et al., 2016)

Lately, Piezo proteins have been shown to play an important role in the context of mechanic nociception, too (Coste et al., 2010). Forming a family of mechanical gated excitatory ion channels, Piezo homologs can be found in vertebrates as well as invertebrates. Mammals express two Piezo genes – Piezo1 & 2 – which are expressed in various tissues, highlighting a potential contribution to mechanosensation in these cells (Zhang et al., 2019).

1.1.2 Nociception in *Drosophila melanogaster*

As described before, nociception is the perception of noxious stimuli, which may potentially cause harmful injuries. This will result in behavioral escape responses to protect the organism from (further) tissue damage. These escape responses can be observed in vertebrates as well as invertebrates (Sneddon, 2004; Hwang et al., 2007; Sillar et al., 2016).

Escape behavior in *Drosophila* was first described during observations of small parasitic wasps *Leptopilina boulardi* rushing after fly larvae. In this attack, female wasps penetrate the larval cuticle with their sharp ovipositor and lay eggs inside the body in order to serve their offspring (Carton et al., 1986). To escape such dangers, *Drosophila* larvae produce a stereotyped defensive behavior in response to noxious stimuli including harsh mechanical stimulation, noxious heat and cold as well as noxious chemicals [reviewed in (Milinkeviciute et al., 2012)]. The unique pattern of escape locomotion elicited by noxious stimulation causes larvae to roll in a corkscrew-like manner (Tracey et al., 2003; Hwang et al., 2007). During the last few years, studies that extensively investigated this topic, led to a more detailed understanding of the physiological and molecular basis underlying nociceptive perception (Kim et al., 2012; Guo et al., 2014; Hu et al., 2018).

Today, nociceptive circuits have been partially unraveled. They start within the peripheral nervous system (PNS) by receiving a noxious stimulus, processing of information in the central nervous system by second and higher order neurons to the point of generating the stereotypic corkscrew-like escape behavior (Figure 2) (Chin et al., 2017; Yoshino et al., 2017). This work focuses on the first step in nocifensive behavior namely the integration

of sensory stimuli by peripheral sensory neurons, which will be introduced in detail in the following chapter.
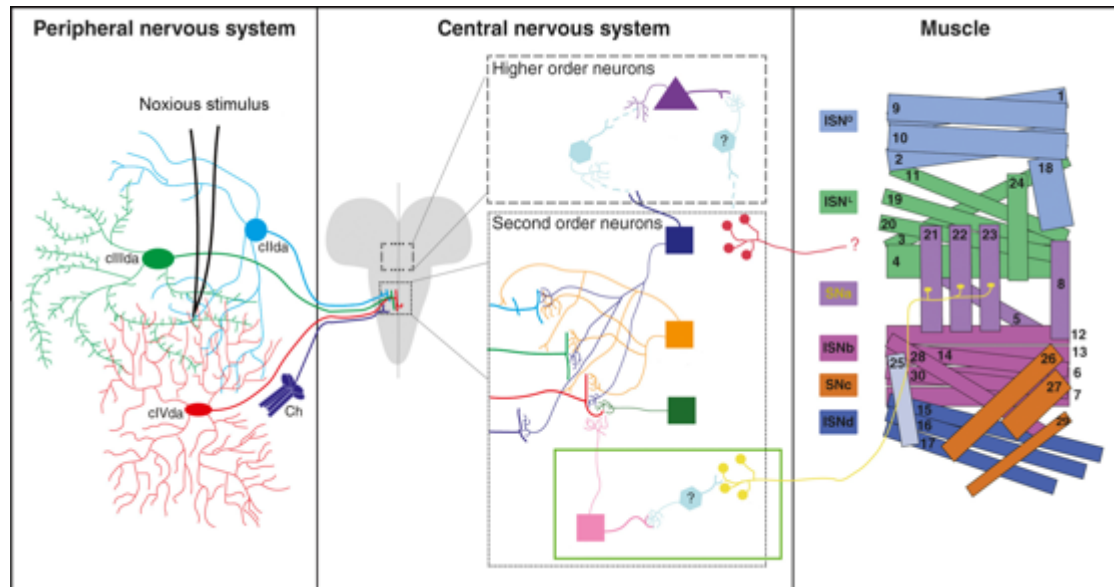
Figure 2. Schematic overview of currently described neurons and neuronal circuits involved in generating the appropriate escape behavior in *Drosophila* larvae. Upon noxious stimulation, sensory neurons within the PNS are activated and send signals to the CNS where they get processed by second and higher order neurons. Finally, the stereotypic nocifensive corkscrew-like rolling pattern is generated via muscles innervated by motor neurons that project through different segmental nerve bundles (ISND, ISNL, ISNd, ISNb, SNa, SNc). Modified from (Chin et al., 2017).

1.1.2.1   Multidendritic sensory neurons of *Drosophila* larvae

The PNS of *Drosophila* larvae is composed of bilateral symmetric and segmentally repeated sensory neurons covering the complete body wall (Figure 3A). Each hemisegment hosts 44 sensory neurons that can be categorized into Type I or Type II neurons, based on their characteristic dendritic morphology (Bodmer et al., 1989; Grueber et al., 2006). On one hand, Type I sensory neurons include monopolar dendrites of external sensory organs as well as chordotonal organs (ChO), which are responsible for e.g. sensing gentle touch and sound (Scholz et al., 2015, 2017). On the other hand, Type II sensory neurons show multidendritic (md) branching patterns. They are further divisible into bipolar dendrite (bd), tracheal dendrite (td) and dendritic arborization (da) neurons (Bodmer et al., 1989; Grueber et al., 2003, 2006; Singhania et al., 2014). Patterning of da neurons has been studied comprehensively by Jan & Jan and coworkers. Thus, among these 44 sensory neurons per abdominal segment, 15 da neurons can be found (Figure 3B) whereby each of those 15 da neurons can be divided in four distinct

subtypes - class I to IV (C1da, C2da, C3da and C4da). The four classes of da neurons have a unique morphology. From class I, which possess very simple dendritic branches to class IV with quite elaborate dendritic arbors (Figure 3C) (Grueber et al., 2006). Even though da neurons show almost complete dendritic field coverage (Figure 3D), overgrowing or crossing of dendrites is prohibited. This repulsion between dendrites of neighboring neurons of the same class leads to "tiling", a phenomenon first described in the retina of cats in 1981 (Wässle et al., 1981). This function is presumed to ensure complete and non-redundant coverage of the receptive field (Grueber et al., 2003; Parrish, 2016). Being morphologically different, da neurons can also be distinguished on the functional level. While class I neurons were shown to be involved in locomotion and presumed to function as proprioceptors (Hughes et al., 2007; Cheng et al., 2010), little is known about class II neurons so far. However, there is some evidence that they are sensitive to gentle touch (Tsubouchi et al., 2012). Class III neurons were identified as receptors for non-noxious mechanical stimuli (Yan et al., 2013) and class IV neurons as polymodal nociceptors sensing noxious temperatures, harmful intense light of short wavelength and harsh touch (Hwang et al., 2007; Xiang et al., 2010; Guo et al., 2014; Kim et al., 2014).
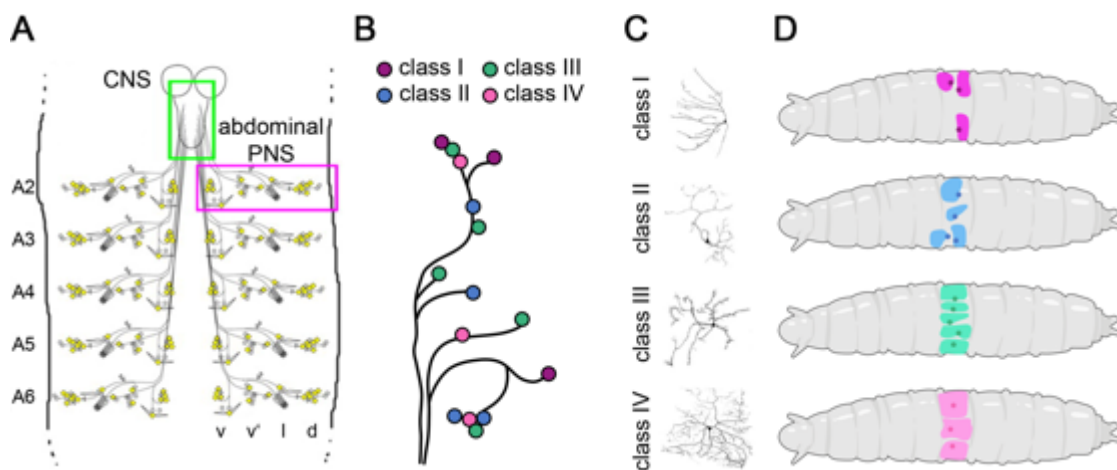
Figure 3. Anatomy and morphology of sensory neurons in the larval PNS. (A) Schematic representation of the abdominal PNS. Sensory neurons are arranged in ventral (v), ventral'(v'), lateral (l) and dorsal (d) clusters [modified from (Grueber et al., 2006)]. **(B)** Schematic of arrangement of all da neuron cell bodies in a single abdominal hemisegment. da neurons of the same color correspond to the same morphological class. [data derived from (Singhania et al., 2014)] **(C)** Representative dendritic morphologies of da neurons. Class I and II neurons have simple dendrites, class III neurons have numerous short dendritic spine-like extensions from their main trunks while class IV neurons have highly branched dendrites. [modified from (Grueber et al., 2006)] **(D)** Shaded areas indicate territory covered by dendric arbor of different da neurons along the larval body wall. The pattern shown is repeated in each abdominal hemisegment [data derived from (Singhania et al., 2014)].

1.1.2.2 Type II Class IV multidendritic neurons and their role in nociception

While the escape response of *Drosophila* larvae upon wasp attack is very striking, little was known about the physiological mechanisms behind, until Tracey and co-workers described that type II class IV multidendritic neurons are necessary and responsible for eliciting this behavior (Hwang et al., 2007). Furthermore they showed that C4da neurons function as polymodal nociceptors that are required for escape behavior provoked by noxious temperatures (≥ 38 °C) (Tracey et al., 2003) and noxious touch (local mechanical stimulation > 30 mN) (Hwang et al., 2007; Zhong et al., 2010).

Several studies have suggested an essential role of different ion channels in mechanotransduction and their results will be described in the following (Table 1). The degenerin/epithelial Na+ channel (DEG/ENaC) gene family, known as *pickpocket* (ppk) genes in *Drosophila*, with 23 reported alleles (Zelle et al., 2013), are specifically expressed in nociceptive C4da neurons (Adams et al., 1998). Here, ppk (also known as ppk1) is required for mechanical nociception but not for thermal nociception. While ppk mutant larvae display strongly reduced nociceptive behavior in response to noxious mechanical stimuli, they exhibit normal behavioral responses to gentle touch (Zhong et al., 2010). Recently, ppk26 (alternatively CG8546 or balboa) – another member of the ppk gene family – was also identified as being required for mechanical nociception (Gorczyca et al., 2014; Guo et al., 2014; Mauthner et al., 2014).

A short time ago, it was found out that mammalian Piezo1 and Piezo2 are mechanically activated channels that mediate touch as well as indirectly suppress mechanical pain responses in mice (Zhang et al., 2019). Evolutionarily conserved, these genes encode for proteins of the Piezo transmembrane protein family. Within the genome of *Drosophila,* a single member of Piezo (DmPiezo) is known (Coste et al., 2012; Moroni et al., 2018). Cell specific knockdown of piezo in C4da neurons results in a drastically reduced nocifensive response of *Drosophila* larvae. Interestingly, analysis of *ppk*, *piezo* double mutants show an further reduction of nociceptive behavior suggesting that both proteins function in two parallel pathways (Kim et al., 2012).

Furthermore, a genetic screen for mutants showing deficits in noxious response identified the *painless* gene, which is required for both thermal and mechanical nociception, but not for sensing gentle touch (Tracey et al., 2003). The painless gene encodes a protein of the

TRP ion channel family (compare chapter 1.1.1). A protein function most closely related to Painless is NOMP-C (no mechanoreceptor potential C), a member of the TRPN family, which was identified as a mechanotransduction channel for gentle touch with high expression patterns in class III but not in class IV md neurons (Cheng et al., 2010; Yan et al., 2013). A further member of the TRP ion channel family identified as an important nociceptor is TrpA1 (transient receptor potential cation channel A1). In larval as well as in adult *Drosophila* TrpA1 functions as a sensor in response to noxious temperatures and chemical exposure (Kwan et al., 2009; Kim et al., 2010; Neely et al., 2011; Khuong et al., 2019)

Table 1. Peripheral sensory neurons, assumed sensory modalities as well as involved genes. Above described peripheral sensory neuron types and representative morphology (not to scale). Sensory modalities mediated by those and genes involved outlined lately. Class I-III md neuron morphology modified from (Grueber et al., 2006).

Peripheral sensory neurons

	Type I	Type II			
Neuron class	**Chordotonal sensory organs**	**Class I**	**Class II**	**Class III**	**Class IV**
Morphology					
Sensory modalities ***genes* involved**	Mechano-sensation *dCirl, nan, iav*	Gentle touch *NompC*			Mechanical nociception *painless, ppk1& 26, piezo*
	Locomotion *NompC*	Proprio-ception		Cold avoidance *painless, NompC, Trpm*	Thermal nociception *painless, TrpA1*
	Cold avoidance *NompC*	Loco-motion			

1.2 Neuropathy models in larval *Drosophila*

Peripheral neuropathy is characterized by degeneration of peripheral motor, sensory and/or autonomic axons, leading to distal muscle weakness, sensory deficits and/or autonomic dysfunction (Schmidt, 2011; Bussmann et al., 2017; Herr et al., 2017; Jarosch et al., 2018). In contrast, drug induced peripheral neuropathies (IPN), e.g. as side effect of chemotherapeutics, are different from injury or mechanical IPN effects (Brace et al., 2017). While drug IPN ubiquitously affect cells irrespective of tissue type, mechanical IPN (e.g. nerve crush or laser axotomy) manifests locally precise effects in tissue or even in single cells.

Drosophila models for mechanical IPNs and several drug induced IPNs have led to scientific findings about axonal degeneration as well as regeneration effects and their underlying molecular mechanisms [for detailed reviews (Brace et al., 2017; Bussmann et al., 2017; Sapar et al., 2019)]. Likewise, forward genetic screens conducted in *Drosophila* have predictive value for the discovery of homologous mammalian genes involved in neuropathy and pain along with the identification of therapeutic drugs for concerning diseases (Bussmann et al., 2017).

1.2.1 Drug induced neuropathy

While the efficacy of cancer treatment has improved over the recent years, toxic side-effects of applied chemotherapeutics still remain a limiting factor for e.g. the applicable dose (Argyriou et al., 2014; Fukuda et al., 2017). In order to overcome this, drug IPN models are suitable techniques and can be applied with ease in *Drosophila* (Bhattacharya et al., 2012). The most common used chemotherapeutics, such as taxane (Taxol/Paclitaxel), platinum agents (e.g. Cisplatin and Oxaloplatin) and proteasome inhibitors (e.g. Bortezomib) can cause neuropathy via diverse mechanisms (Cashman et al., 2015; Fukuda et al., 2017). Taxane compounds bind to microtubules to inhibit axonal transport mechanisms as well as preventing microtubule depolymerization (Jordan et al., 2004; Beliu et al., 2018). By forming DNA adducts, platinum based drugs lead to cell cycle arrest (Johnstone et al., 2014) while Bortezomib, a candidate of a novel class of

chemotherapeutics, acts via proteasome inhibition resulting in protein accumulation and finally apoptosis (Adams, 2004; Tsakiri et al., 2017).

Applying Taxol in a *Drosophila* model, peripheral neuropathy can be observed (Figure 4) and various molecules involved in the degeneration process were described (Bhattacharya et al., 2012). Among them is NMNAT (nicotinamide mononucleotide adenylyltransferase), typically known for its enzymatic function during NAD+ (nicotinamide adenine dinucleotide) synthesis. Overexpression of NMNAT – which has three orthologs in humans MNAT1-3 (Brazill et al., 2018) – or a loss of *wallenda* (a *Drosophila* ortholog of the vertebrate dual leucine zipper kinase) protects neurons from degeneration (Bhattacharya et al., 2012).

Since Taxol causes dose limiting neuropathy in human cancer patients, the destructive effects on nerve morphology were investigated in detail, employing *Drosophila* models (Stillman et al., 2008; Bhattacharya et al., 2012; Fukuda et al., 2017; Brazill et al., 2018; Hamoudi et al., 2018). Thus, it was shown that different pronounced phenotypes of nerve degeneration occur due to Taxol treatment. Beside severe impact on cell anatomy, including complete loss of axons and dendrites of C4da neurons (Figure 4C, C`), intermediate mild phenotypes can be observed, marked by axonal swellings, buddings and fragmentation (Figure 4B, B`) (Bhattacharya et al., 2012). In contrast, dimethyl sulfoxide (DMSO) treated animals show unperturbed C4da morphology pattern (Figure 4A, A`). Interestingly, investigations on the neuromuscular junction (NMJ) of larval *Drosophila* demonstrated no disruption, neither pre- nor postsynaptic, indicating that Taxol IPN does not cause synaptic instability (Bhattacharya et al., 2012). Antecedent characteristics of IPN in *Drosophila* are hallmarks of mammalian axonal degeneration as well, highlighting the alienability of invertebrate and vertebrate IPN models [reviewed in (Coleman, 2005)].
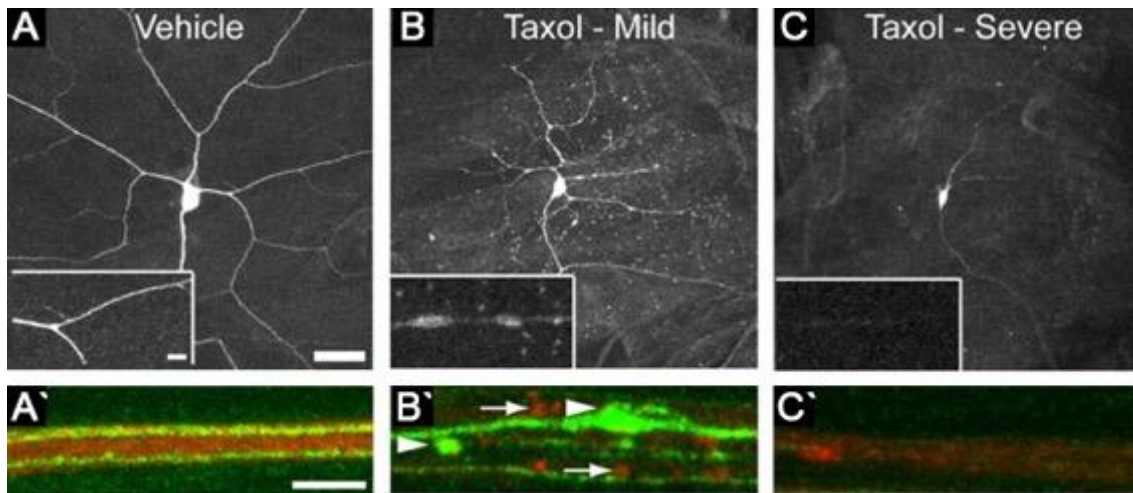
Figure 4. Peripheral neuropathy can be observed in *Drosophila* larva following Taxol treatment. (A – C) Dendrites and cell bodies of C4da neurons in vehicle (DMSO) or 30 µM Taxol treated animals. Swellings/deformations or loss of dendritic arbores during Taxol presence are detectable (inserts). Scale bar 30 µm, Inserts 6 µm. **(A` – C`)** Segmental nerve between abdominal hemisegment A3 and A4 is visualized in red (Cy3-HRP; labels neuronal membranes) while in green (*ppkEGFP*) a subset of sensory neurons is labelled. Three peripheral nerves can be observed in the vehicle, while distorted nerves with prominent swellings and fragmentation are distinguishable – within EGFP (arrowheads) and HRP (arrows) – following Taxol treatment. Scale bar: 5 µm. Modified from (Bhattacharya et al., 2012).

1.2.2 Mechanically induced neuropathy

Xiong and co-workers described a simple and easy to achieve nerve crush model (Figure 5) (Xiong et al., 2010) that is in many aspects compatible with the mammalian sciatic nerve crush injury model (Reinhold et al., 2015). In the living animal, the segmental nerves, located on the ventral side of the larva under the cuticle, can be gently crushed with forceps. The segmental nerves include sensory as well as motor neurons orientated bidirectional. Thus degeneration and/ or regeneration processes on the site of injury can be observed over time in both cell types simultaneously (Stone et al., 2010; Xiong et al., 2010, 2012). With the help of the nerve crush assay, the role of the MAP kinase JNK (Jun N-terminal kinase) in axons injury and regeneration has been studied and findings concerning *wallenda* were confirmed (Brace et al., 2017). Xiong and co-workers showed that within a few hours after nerve crush, the JNK phosphatase *puckered* (puc) is upregulated, whereby it regulates injury-induced transcriptional changes (Xiong et al., 2012).
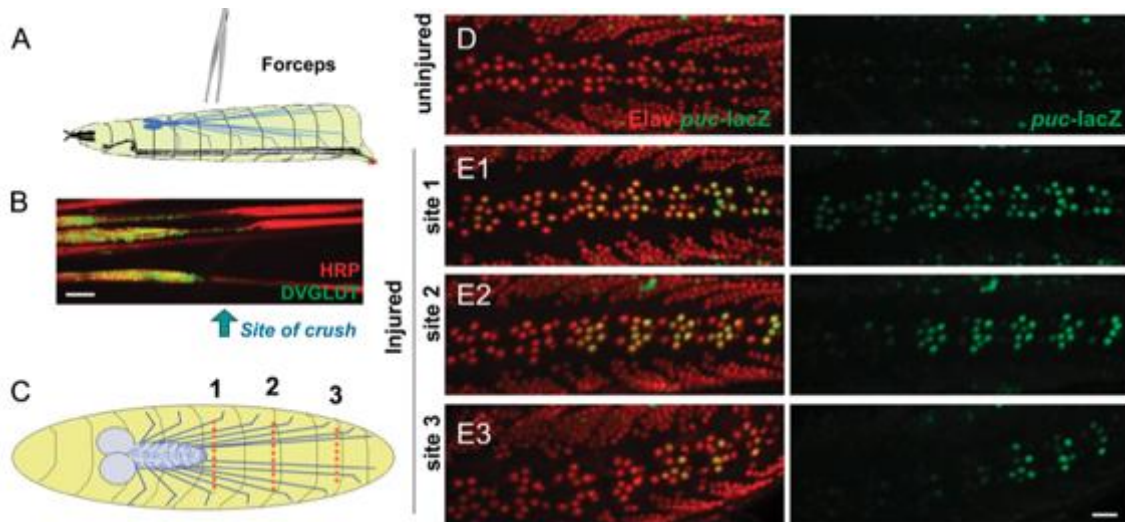
Figure 5. Mechanical induced neuropathy due to a nerve crush assay. (A) Schematic of the nerve crush assay described 2010 by Collins and co-workers. **(B)** Injured segmental nerves after 24 h. **(C)** Different crush sites (dashed red lines) injure a predictable number of motoneurons – cell bodies marked with blue dots. **(D – E)** In uninjured animals, puc expression is barely detectable. A nuclear localization signal on lacZ (green) localizes the reporter to the nucleus and neuronal nuclei are detected by staining for the Elav (embryonic lethal abnormal vision) (red) marker. **(E 1 – 3)** Injuries at sites 1–3 initiate expression of *puc* in a defined subset of motoneuron cell bodies as predicted in **(C)**. Scale bar: 25 μm. Taken from (Xiong et al., 2010).

1.3 Adhesion class G-Protein coupled receptors

Adhesion class G-protein coupled receptors (aGPCRs), with 33 constituent members, is the second largest group within the GPCR family. They share structural features with all other representatives of this receptor family including a seven-transmembrane (7TM) domain, an extracellular N terminus as well as an intracellular C terminus (Krishnan et al., 2016). They are presumed to have a dual role, in which they act as cell-surface molecules, mediating cell-cell-contacts on one side and function as classical receptors, activating second messenger pathways inside the cell and finally, a cellular response, on the other side. (Pierce et al., 2002; Langenhan et al., 2013; Aust et al., 2016). Activation of aGPCRs occurs through a highly diverse range of molecules like light-sensitive compounds, calcium, hormones, neurotransmitters and others making these receptors very interesting but difficult to study (Bockaert, 1999; Araç et al., 2016; Liebscher et al., 2016; Nijmeijer et al., 2016). Unsurprisingly, given the variety of activating stimuli, aGPCRs are involved in many physiological processes and hence they are appropriate targets for pharmaceutical drugs (Flower, 1999; Lundstrom, 2006; Basith et al., 2018; Purcell et al., 2018; Langenhan, 2019).

In spite of being an expansive receptor group, the physiological function of aGPCRs is poorly understood. This might be caused by the fact, that a majority of aGPCRs ligands and interaction partners are unknown. Nevertheless, many of their structural features have been well characterized over the last decades. All aGPCRs are heterodimers consisting of a long extracellular adhesion subunit and GPCR-like transmembrane spanning regions. In humans there are 33 adhesion class receptors grouped into nine different families according to the similarity of their 7TM domains and N-terminal domain architecture (Langenhan et al., 2013; Nijmeijer et al., 2016) (Figure 6A). A further characteristic of aGPCRs is the GPCR proteolysis site (GPS) located close to the 7TM domain. The GPS (~ 40 amino acids) is part of the much larger GPCR autoproteolysis inducing (GAIN) domain consisting of approximately 320 amino acid residues. Deletion experiments demonstrated, that the entire GAIN domain is both required and sufficient for autoproteolysis (Nieberler et al., 2016).

Latrophilins, a group of prototypic aGPCRs, are present in the invertebrate as well as in the vertebrate genome. This indicates high evolutionary conservation among the receptor family (Fredriksson, 2005; Kovacs et al., 2016). Therefore, these receptors provide a

perfect target to study aGPCRs biology and compare among organisms. The mammalian genome contains three latrophilin homologs (LPHN1 - 3), *C. elegans* has two (LAT-1 and LAT-2) and in *Drosophila melanogaster* one homolog (dCIRL) can be found (Figure 6B). As a characteristic feature of aGPCRs, Latrophilin consists of three major regions: (i) a long extracellular N-terminal region comprising a rhamnose binding lectin-like domain (RBL), a hormone binding domain (HRM) and an olfactomedin-like domain (OLF), (ii) the 7TM helix region with the close located GPS and GAIN domain and (III) a short intracellular C-terminal fragment (CTF). (Langenhan et al., 2013; Araç et al., 2016)
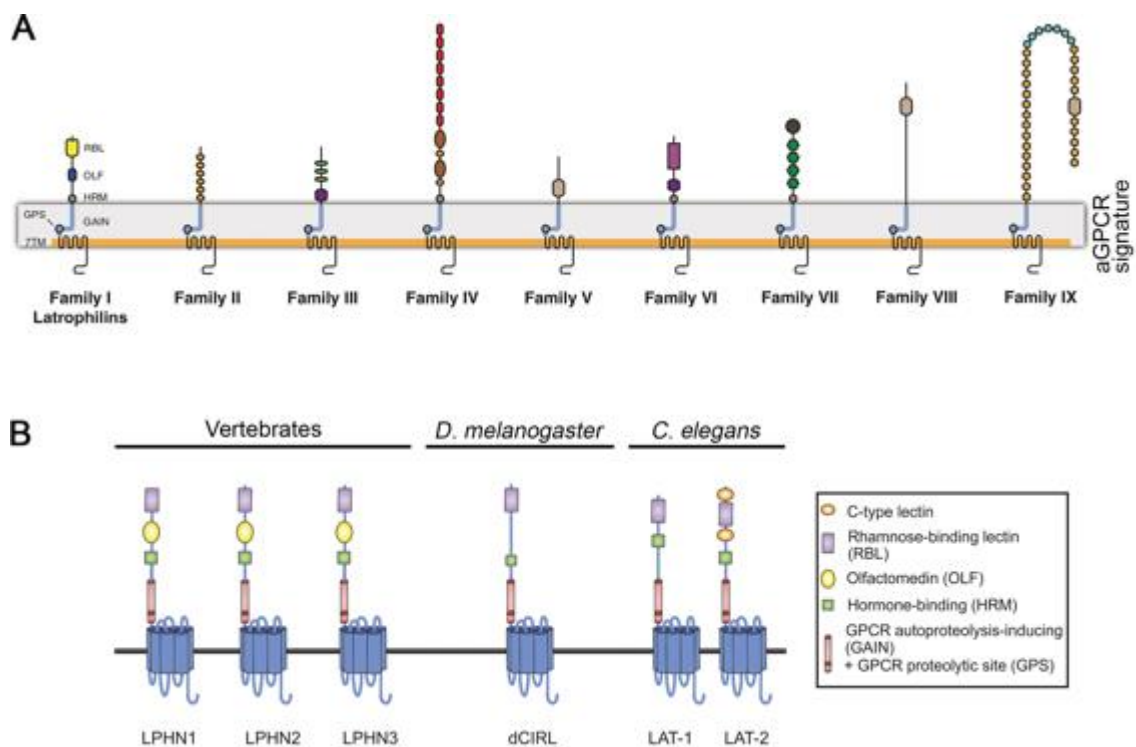
Figure 6. Adhesion-GPCR families and structural layout of Latrophilins in vertebrates and invertebrates. The aGPCRs are subdivided in 9 distinct families, which all share a specific aGPCR signature (GAIN and 7TM domain) but are distinguished by unique combination of NTF domains **(A)** [modified from (Langenhan et al., 2013)]. **(B)** Molecular layout of Latrophilin / CIRL: Vertebrates LPHN1-3, *Drosophila* dCIRL and *C. elegans* LAT-1 and LAT-2 [modified from (Schöneberg et al., 2019)].

1.3.1 Cirl function in mammals

Originally, mammalian LPHN1 was identified based on its ability to bind alpha latrotoxin (α-LTX), a neurotoxin naturally found in the venom secreted by the black widow spider (Davletov et al., 1996; Krasnoperov et al., 1997). The Ca2+ independence of this interaction led to the alternative nomenclature CIRL (Ca2+ independent receptor of latrotoxin (Krasnoperov et al., 1997). The mammalian Latrophilin subfamily comprises three homologs (LPHN1-3) (compare chapter 1.3) LPHN1 and LPHN3 are predominantly expressed in the CNS, while LPHN2 is rather commonly distributed (Ichtchenko et al., 1999; Röthe et al., 2019). LPHN3 has been associated with attention deficit hyper-activity disorder (ADHD), a common psychiatric disorder (Arcos-Burgos et al., 2010; Domené et al., 2011). Furthermore, in various family-based studies, aGPCRs have been identified/suggested to cause immune responses (e.g. allergies), inflammation, diseases of the respiratory system (chronic and reversible airflow obstruction), tumorigenesis and insulin release. Moreover, an involvement in surfactant control, muscle hypertrophy, myelination, mast cell degranulation and proprioception have also been reported (Figure 7) (Kovacs et al., 2016; Langenhan et al., 2016; Scholz et al., 2016; Lin et al., 2017; Purcell et al., 2018; Scholz, 2018; Röthe et al., 2019).
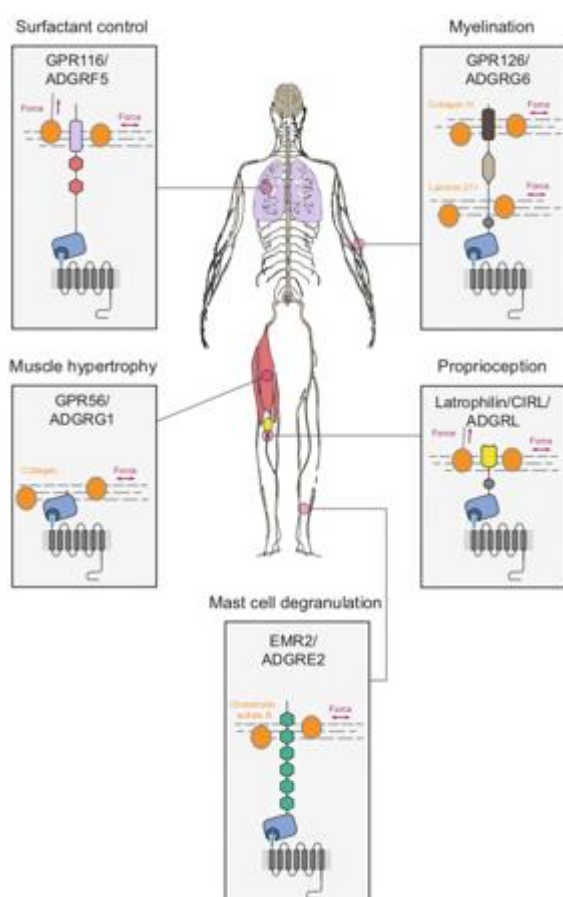
Figure 7. Adhesion GPCRs in mechano-sensation. aGPCRs have been suggested to be involved in mechanosensation / proprioception as well as in surfactant control, myelination, muscle hypertrophy and mast cell degeneration. Adapted from (Scholz et al., 2016).

1.3.2 Cirl function in *Drosophila*

However, only recently first physiological aspects of dCIRL function were shown by establishing a genetic dCirl toolkit in *Drosophila* – including knockout, loss of function, UAS/GAL4 fly lines and labelled constructs. Here, dCIRL was shown to shape the response of larval pentascolopidial ChO (lch5) neurons (type I sensory neurons) upon mechanical stimulation (Scholz et al., 2015). Knockout animals exhibited abnormal crawling patterns in *Drosophila* larvae, which could be rescued by cell-specific *dCirl* reexpression experiments. Moreover, *dCirl*KO larvae are less responsive to gentle touch. Interestingly morphological analysis of lch5 chordotonal organs revealed not alteration due to the loss of function of the aGPCR. Electrophysiological recordings confirmed that dCIRL acts in mechanosensory neurons by modulating ionotropic receptor currents (Figure 8). As an intracellular mechanism, cAMP quenching through dCIRL is responsible for increasing mechanosensation of lch5 neurons (Scholz et al., 2017).
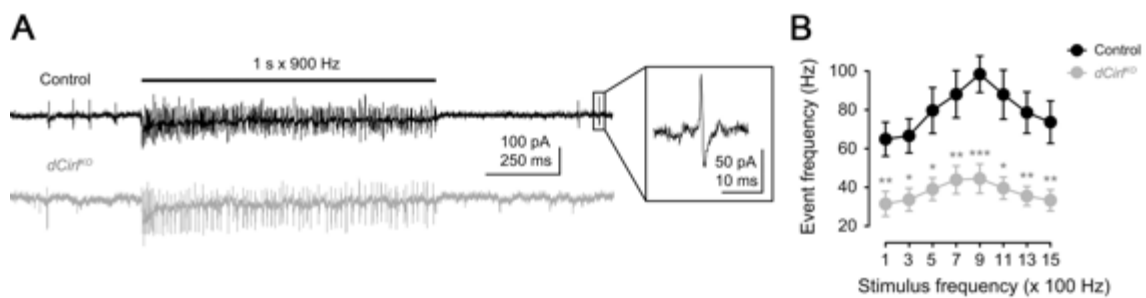
Figure 8. dCIRL shapes mechanosensation in *Drosophila* larval lch5 neurons. (A) Representative electrophysiological recordings from lch5 axons of control and *dCirl*KO mutants during 900 Hz mechanical stimulation. **(B)** Evoked action currents quantified – for control and knockout animals respectively – show highest frequencies at 900 Hz but are drastically diminished in mutant larva. Modified from (Scholz et al., 2015).

In order to reveal if the previously described autoproteolysis property of aGPCRs or the uncovering of the receptor's tethered agonist (*Stachel*) – which begins at the GPS and can stimulate receptor activity (Liebscher et al., 2014b, 2016) – may be required for proper mechanosensation of lch5 neurons in *Drosophila*, Scholz and coworkers employed different proteolysis deficient mutants. Autoproteolytic activity of the GAIN domain was suppressed in two sets of dCirl alleles, *dCirl*H>A and *dCirl*T>A, in which the latter is within the *Stachel* sequence. Morphological investigations revealed autoproteolysis activity is not needed for proper membrane targeting within the chordotonal organs. But receptor currents were affected in different manners. While *dCirl*H>A mutants displayed wildtype

responses to 900 Hz mechanical stimulation, the *dCirlT>A* mutant delivered a dCirlKO phenotype. This suggests that in the chordotonal organs, dCIRL activation depends on an intact *Stachel*, but NTF-CTF disruption is not relevant (Scholz et al., 2017).
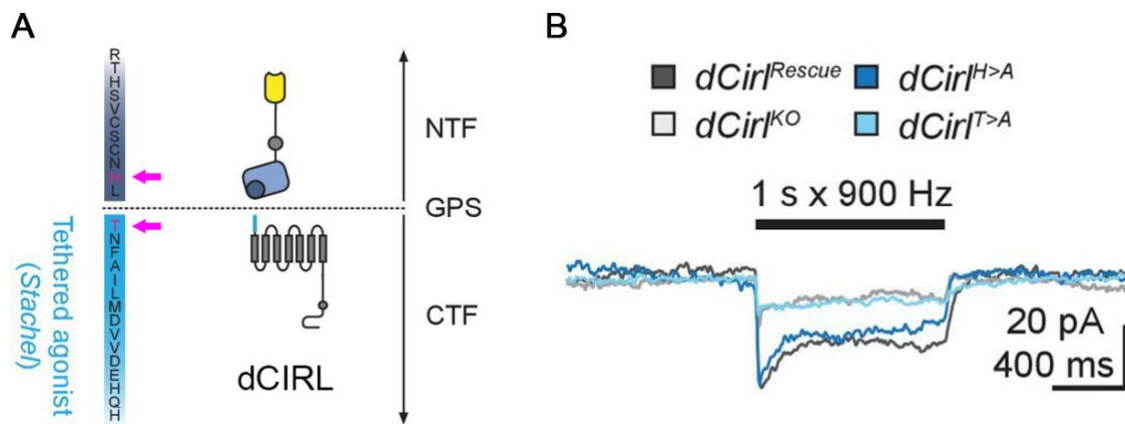
Figure 9. GPS mutations reveal differential effects on mechanosensation in lch5 neurons.
(A) Structure of the dCIRL GPS region. The CTF component hosts the tethered agonist (*Stachel*) sequence, proven to act as a agonist in many aGPCRs (light blue) (Liebscher et al., 2014b, 2016). Magenta: conserved, mutated residues that are necessary for GPS cleavage. **(B)** Electrophysiological receptor current recordings of lch5 neurons under TTX inhibition exhibit the divergent effects of the GPS mutations on mechanosensation. Modified from (Scholz et al., 2017).

But still, information about possible interaction partners of dCIRL remain vague. Due to recent reports, some molecular candidates arouse suspicion to be potential interactors e.g. cation channels deriving from the highly conserved TRP channel families like *nompC* (no mechanoreceptor potential C), *nan* (nanchung) or *iav* (inactive) (Padinjat, 2004; Montell, 2005). Furthermore, Teneurins (TEN), which are evolutionary conserved molecules that play a major role in axon guidance and synapse formation, were recently supposed to interact with Latrophilins (Li et al., 2018).

2 Motivation of the study

This study set out to characterize the *in vivo* function of Latrophilin/CIRL in the aspect of nociception employing larval *Drosophila melanogaster*. Latrophilin has been proven to act in a variety of physiological processes in different species: synaptic transmission and connectivity (Südhof, 2001; Sando et al., 2019), development (Langenhan et al., 2009), fertility (Prömel et al., 2012), defects of the nervous system, allergies and cancer (O'Hayre et al., 2013; Boyden et al., 2016; Langenhan et al., 2016). In *Drosophila*, Latrophilin function was recently associated with mechanosensation of gentle touch and sound (Scholz et al., 2015, 2017). However, we still lack basic knowledge to describe the precise physiological role of *dCirl* sufficiently.

This work focuses on the molecular mechanisms of CIRL activity in larval sensory neurons (type II class IV da neurons). To this end, *Drosophila* mutants were employed and behavioral paradigms, fluorescence microscopy as well as optogenetic approaches were applied. Furthermore Ca^{2+}-imaging was carried out to obtain information about C4da-neuron activity during nocifensive stimulation in wildtype and knockout animals. In addition, CIRL function was studied in a pathological context by employing a drug induced neuropathy model. Experiments measured mechanosensory signal transduction and progression of pathology following the induction of peripheral neuropathy in *Drosophila* larvae. In combination these approaches shed light on the function of the adhesion-GPCR Latrophilin/CIRL in nociception and neuropathy.
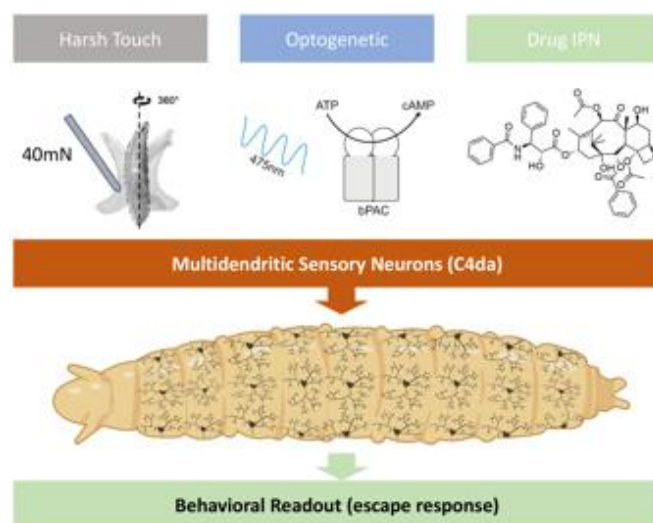
Figure 10. Graphical abstract of approached methods and readout. This thesis focusses on sensory neurons (C4da) by employing noxious mechanical stimuli in combination with the optogenetic tool bPAC to manipulate second messenger pathways. Furthermore, CIRL function was analyzed in a pathological context via a drug (Taxol) IPN model.

3 Materials and Methods

3.1 *Drosophila melanogaster*

Drosophila melanogaster, the common fruit fly, has been used successfully for over 100 years to study a variety of biological processes. Meanwhile, *Drosophila* has become one of the most powerful organisms in experimental research (Dahmann, 2008).

Figure 11A shows the life cycle of flies raised at 25°C. Out of fertilized eggs (~ 0.5 mm long), larvae will hatch after ~ 24 h to develop to first, second (1 day each) and third instar larvae (1 – 2 days). After the 3rd instar larval stage, changes in morphology and physiology occur during pupation. Eclosion takes place on day 9 - 10. After flies reach sexual maturity, the cycle begins anew. By increasing/decreasing the temperature, the life cycle of *Drosophila* can be accelerated/decelerated (Ashburner et al., 2007; Dahmann, 2008).

One advantageous aspect of working with the fruit fly is certainly the large diversity of elaborate genetic tools like the binary GAL4/UAS system (Figure 11B), which originally derives from yeast, the related LexA/LexAop and QF/QUAS systems (Johnston, 2002; Lai et al., 2006; Dahmann, 2008; Potter et al., 2010). These allow ectopic gene expression as well as strategies to reduce gene expression (e.g. RNAi) in almost any cell or tissue of interest (Brand et al., 1993; Montgomery et al., 1998; Dietzl et al., 2007; Ni et al., 2009; Paul et al., 2015).
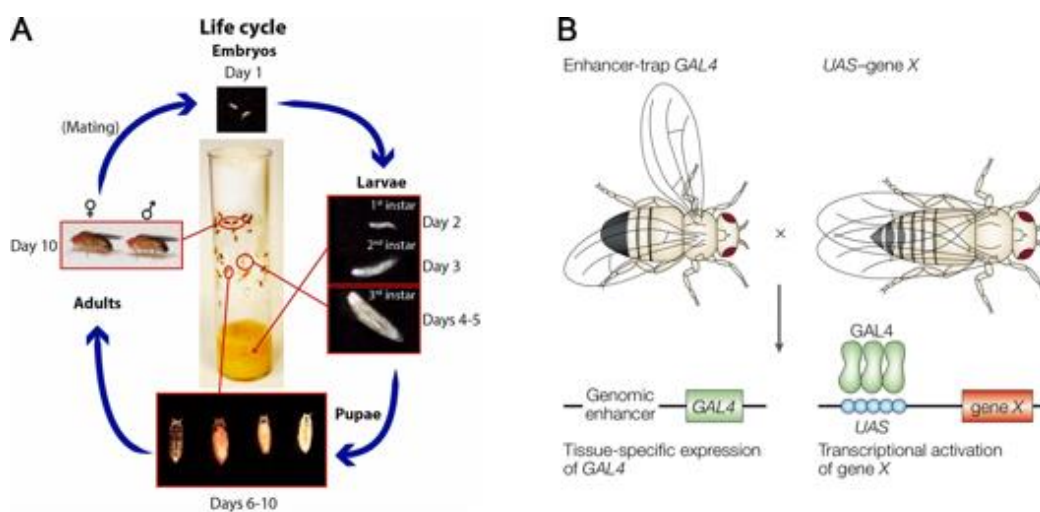
Figure 11. *Drosophila melanogaster*. (A) Life cycle of *D. melanogaster* at 25°C [modified from (Hales et al., 2015)]. **(B)** The binary UAS/GAL4 system for direct gene expression or tissue specific gene knockdown [adapted from (Johnston, 2002)].

3.1.1 Fly cultivation and handling

Drosophila stocks and crosses were, if not mentioned otherwise, raised at 25 °C on standard cornmeal food (Table 2) with light-dark-cycle (LD) 12:12.

Table 2. Recipe for standard fly-food used in this study.

standard cornmeal food	
1 l	H_2O
4.5 g	Agar
20 g	beet syrup
72.2 g	malt
9 g	soy flour
16.3 g	yeast
72.2 g	corn flour
1.45 g	nipagine
5.7 g	propionic acid

3.1.2 Fly stocks

Transgenic fly strains used in this study are listed below (Table 3). Stocks ordered from Bloomington Stock Center (BDSC; Bloomington, USA) are indicated with corresponding stock ID as well as RNAi strains purchased from Vienna *Drosophila* Research Center (VDRC; Vienna, Austria) or Fly Stocks of National Institute of Genetic (NIG-fly; Shizuoka, Japan).

Table 3. Fly strains used in this study.

Name	Genotype	Shorthand	Reference
RJK 000	*w[1118]*	w_{1118}	
RJK 188	*w[1118]; UAS-bpac/CyO w-GFP (w[-])*	bPAC	(Stierl et al., 2011)
RJK 290	*y[1] w[1] dnc[ML] f[36a]/ FM7a*	dunce$_{ML}$	(Salz et al., 1984) BDSC#9407

RJK 461	*cantonS*	Canton-Special	(Lindsley et al., 1968)
RJK 584	*w[*]; P{w[+mC]=ppk-GAL4.G}2*	C4da driver II	(Zhong et al., 2010) BDSC#32078
RJK 586	*w[*];+; P{w[+mC]=ppk-GAL4.G}3*	C4da driver III	(Zhong et al., 2010) BDSC#32079
RJK 592	*;;UAS-GCamp6::mCherry*	GCamp6	Gift from Venkatachalam K.
RJK 620	*dCirl[KO]/CyO w-GFP(w-);UAS-GCamp6-mCherry/TM6B,Tb*	GCamp6, dCirl[KO] background	
RJK 662	*w[1118]; Cirl[108/3A.2]{attP+ loxP+}[w-] / CyOGFP(w-); ppk-GAL4 / TM6B,Tb*	dCirl[KO]; C4da driver	
RJK 666	*w1118; + ; P{ppk-CD4-tdGFP}8/TM6B, Tb*	C4da marker (green)	(Han et al., 2011) BDSC#35843
RJK 686	*w[1118]; P{w[+mC]=ppk-CD4-tdGFP}1b*	C4da marker (green)	(Han et al., 2011) BDSC#35842
RJK 687	*w1118; P{ppk-CD4-tdTom}4a; +*	C4da marker (red)	(Han et al., 2011) BDSC#35844
RJK 695	*w[1118]; phiC31{KK108383}v100749; +*	dCirl-RNAi	(Dietzl et al., 2007) VDRC#KK100749
RJK 696	*w[*]; +; P{y[+t7.7] w[+mC]=20XUAS-IVS-mCD8::GFP}attP2*	mCD8::GFP marker	(Pfeiffer et al., 2010) BDSC#32194
RJK 700	*w[1118]; Cirl[108/3A.2]{attP+ loxP+}[w-]/CyO GFP[w-]*	dCirl[KO]	(Scholz et al., 2015, 2017)
RJK 702	*w[1118]; Cirl[108/3A.2]{attP+ loxP+}[w-] att{Cirl-rescue(pTL370) [w-]}[attPLAT]/CyO GFP[w-]; +*	dCirl[rescue]	(Scholz et al., 2015, 2017)
RJK 703	*w[1118]; Cirl[108/3A.2]{attP+ loxP+}[w-] att{Gal4.2::p65d::dCirl [w+]}[attPLAT]/CyOGFPw-*	dCirl[GAL4]	(Scholz et al., 2015, 2017)
RJK 704	*y[1] w[*];; D[*] attP{20xUAS-dCirl::Flag w+}*	UAS-dCirl[Flag]	(Scholz et al., 2015, 2017)
RJK 706	*w[1118]; Cirl[108/3A.2]{attP+ loxP+}[w-] att{dCirl/T742A(pMN9) [w-]}[attPLAT]/CyOGFP; +*	dCirl[(T>A)]	(Scholz et al., 2015, 2017)
RJK 707	*w[1118]; Cirl[108/3A.2]{attP+ loxP+}[w-] att{dCirl/H724A(pMN44) [w-]}[attPLAT]/CyO;+*	dCirl[(H>A)]	(Scholz et al., 2015, 2017)
RJK 715	*Dnc[1]*	dunce[1]	(Salz et al., 1984) BDSC#6020

RJK 717	*f[36a]*	control dnc$_{ML}$	BDSC#43
RJK 757	*w[1118]; dCirl-GAL4/CyoGFPw-; UAS-RFPnls, LexAop-GFPnls[GN112]/TM6B, Tb*	dCirl driver, RFPnls marker	
RJK 773	*w[-]; dCirl[108/3A.2]{attP+ loxP+}[w-]/CyOGFPw-; 20xUAS-dCirl::Flag w+/TM6B, Tb*	Cirl$_{[KO]}$; UAS-dCirl$_{Flag}$	(Scholz et al., 2015, 2017)
RJK 780	*w[1118]; PBac{y[+mDint2] w[+mC]=UAS-CD4-tdTom}VK00033*	UAS-CD4-tdTom	(Han et al., 2011) BDSC#35837
RJK 796	*w[1118]; dCirl-Gal4 / CyOGFP ; ppk-CD4-tdGFP / Tb*	dCirl$_{GAL4}$; C4da marker	
RJK 782	*y[1] w[*]; P{w[+mC]=UAS-CD4-tdTom}7M1*	UAS-CD4-tdTom	(Han et al., 2011) BDSC#35841

3.2 Confocal imaging

3.2.1 Immunohistochemistry and image acquisition

Briefly, immunohistochemistry was performed as previously described (Ehmann et al., 2014; Scholz et al., 2017). 3rd instar *Drosophila* larvae were dissected in ice-cold phosphate buffered saline (PBS), fixed for 10 min using 4 % paraformaldehyde (PFA) in PBS and blocked for 30 min in PBT [PBS with 0.05 % Triton X-100] containing 5 % normal goat serum [NGS; (005-000-001, Jackson ImmunoResearch)]. Preparations were incubated with primary antibodies (in PBT, containing 5 % NGS) at 4 °C over night. After two short and three 20 min washing steps with PBT, secondary antibodies (in PBT, containing 5 % NGS) were added to the fillets and incubated for 2 h at room temperature. This was followed again by two short and three 20 min washing steps with PBT. Samples were mounted in Vectashield (H1000, Vector Laboratories). Primary antibodies were used in the following dilutions: mouse-α-GFP (1:500, Sigma Aldrich), rabbit-α-RFP (1:250, Antikörper-online). Secondary antibodies: α-mouse-AlexaFluor488 (Invitrogen), α-rabbit-Cy3 (Dianova) and HRP-Cy3 (Dianova), were used 1:250 respectively. Images were acquired with a Zeiss LSM5 Pascal system (objective: 63x, NA 1.25, oil) or Leica TCS SP5 system (objective: 20x, NA 0.75, multi immersion; 40x, NA 1.25, oil; 63x, NA 1.40, oil).

Table 4. Recipe for 10x PS stock solution.

10x PBS		
NaCl	74 g	1.06404, Merck
$Na_2HPO_4*2H_2O$	12.46 g	1.06580, Merck
$NaH_2PO_4*H_2O$	4.14 g	1.06345, Merck

Fill up to 1 l with H_2O. For 1x PBS dilute 1:10; pH was adjusted to 7.4 using 1 M NaOH or 1 M HCl. For PB: add appropriate volume (0.05 %) of Triton X-100 (T9284, Sigma Aldrich).

Table 5. Recipe for fixation stock solution.

4 % PFA in 1x PBS		
PFA	8 g	1.04005, Merck
H_2O	150 ml	heat up to 55 °C
2M NaOH	some drops until solution turns clear	1.09136, Merck
10x PBS	20 ml	

Fill up to 200 ml using H_2O; pH was adjusted to 7.4 using 1 M NaOH or 1 M HCl.

3.2.2 Live imaging of multidendritic neurons

Living 3_{rd} instar larvae (96 hours after egg laying (AEL)) were embedded in Glycerol (G9012, Sigma-Aldrich) and mounted on standard microscope slides. Coverslips were held in place with two drops of Korasilon-paste (medium viscosity, Kurt Obermeier GmbH). C4da neurons were imaged by confocal stack microscopy using a Zeiss LSM700 upright microscope and visualized applying *ppk-CD4-tdTomato*, *ppk-CD4-tdGFP* or *ppk$_{GAL4}$ > UAS-CD4-tdGFP*. For comparison, abdominal segment A5 was chosen. For imaging the whole dendritic field of C4da neurons, a 20x, NA 0.8, air objective was used. Step size of stacks varied from 0.5 – 2 μm.

Image acquisition and quantification for morphological analysis of Cirl mutants (Chapter 4.1.3) was performed by our collaborators from the Soba Lab (Chun Hun, Neuronal Patterning and Connectivity, Center for Molecular Neurobiology, University Medical Center Hamburg-Eppendorf (ZMNH)). Image acquisition and quantification for morphological analysis of the IPN model was performed by myself.

3.2.3 Image processing and quantification

Z-projections of confocal stacks, background subtraction and interpolation of images were processed with ImageJ (MacBiophotonics). Background subtraction was carried out manually, while quantification of dendrites of C4da neurons were traced semi-

automatically. The "Filament Tracer module" of Imaris x64 9.1.2 (BitPlane AG, Zürich, Switzerland) was used to describe dendrite morphology. Extracted parameters were: total dendrite length, number of terminals, Sholl analysis and Strahler analysis.

Schematic illustrations, graphics and image labelling were compiled using Adobe Photoshop CC 2019 (Adobe Systems, San Jose, USA).

3.3 Calcium Imaging

3.3.1 Larval preparation and image acquisition

3_{rd} instar larvae (96 h AEL) expressing the genetically encoded Ca^{2+} sensor GCaMP6 were filleted in ice cold hemolymph-like saline (HL-3). Preparations were performed as previously described (Schmid et al., 2008). To improve imaging acquisition quality as well as to stimulate nociceptors through the cuticula, the filets where flipped and mounted dorsal side upwards. C4da neurons expressing GCaMP6 were then imaged using a 20x Olympus XLUMPlanFL N water objective, NA 1.00, attached to an Olympus BX51WI upright microscope.

For all functional imaging experiments, a Cool LED pE-4000 was used for excitation of GCaMP. An irradiation intensity of 289.37 ± 6.38 µW/mm$_2$ at 490 nm was employed. Intensity measurements were obtained with Compact Power and Energy Meter Console PM100D equipped with a Slim Photodiode Power Sensors S130C (Thorlabs GmbH, Dachau, Germany). Image acquisition was performed with an electron-multiplying CCD camera (EMCCD, Ixon+, Andor) which was triggered via VisiView V4.3.0.2 Software (Visitron Systems GmbH, Puchheim, Germany). For recordings, exposure time was set to 75 ms (acquisition rate 13.33 Hz) to obtain fluorescence values within the dynamic range (64-bit) of CCD camera. Spatial resolution was set to full frame (512 x 512 pixels) with a binning (number of points on the chip that will be binned into one digital pixel) of 1 and an EMCCD gain of 300. Automated time-laps series of 400 time points (cumulative 30 s) were recorded. During the time series, force stimulation was applied to the dendritic field of neurons using a manually sealed glass electrode (GB150-8P, inner diameter 0.86 mm, outer diameter 1.5 mm, Science Products), with a tip diameter of ~ 20 µm, that was attached to an automatically controlled micromanipulator (Sensapex uMp-3, Sensapex Oy, Oulu, Finland). The force stimulation protocol was automatically applied via Sensapex PC Suite (v1.95 Win x64) Software using the "Custom Drive Editor" as follows: Select Device > Set Speed (max) > Relative Distance (100 µm in X) > Start Drive > Delay (300 ms) > Set Speed (max) > Relative Distance (- 100 µm in X) > Start Drive. In each preparation one force stimulus was applied to the filleted larva.

All functional imaging experiments were performed in hemolymph-like solution [HL-3; (Ljaschenko et al., 2013)]. 1.5 mM CaCl$_2$ was added to the solution prior to recordings.

Table 6. Recipe for HL-3 stock solution for Ca2+-imaging.

HL-3		
NaCl	70 mM	1.06404, Merck
KCl	5 mM	1.04933, Merck
MgCl2	20 mM	1.05833, Merck
NaHCO3	10 mM	S6297, Sigma Aldrich
D-(+)-Trehalose	5 mM	T5251, Sigma Aldrich
Saccharose	115 mM	S9378, Sigma Aldrich
HEPES	5 mM	54457, Sigma Aldrich
CaCl2	1.5 mM	54457, Sigma Aldrich

pH was adjusted to 7.2 using 1 M NaOH.

3.3.2 Image processing and quantification

Imaging data was processed using ImageJ with StackReg/TurboReg (Ecole polytechnique fédérale de Lausanne) plugin.

Correction for sample movement artefacts was carried out using the "rigid body" mode of StackReg plugin. For each measurement the background was calculated manually (mean fluorescent value of a non-labelled area of 15 frames before stimulus onset) and subtracted afterwards. Cell bodies of individual cells were selected manually as regions of interest (ROIs) in the maximum intensity projections from the time series.

Relative change in fluorescence ($\Delta F/F$) at time point t was calculated as follows:

$$\frac{\Delta F}{F} = \frac{F(ROI)_t - F(ROI)_0}{F(ROI)_0}$$

The average GCaMP intensity from the 15 frames prior to stimulation was used as $F(ROI)_0$ and $F(ROI)_t$ was the fluorescence intensity at each time point t.

The analyzing period was set to 15 frames (1125 ms) prior to stimulation till 27 frames (2025 ms) after stimulation.

For quantification, single traces were compared as well as the mean of all measurements from each genotype were presented ± SEM. Starting point of stimulation was aligned

manually. Peak amplitudes and peak-amplitude-quotient (maximal $\Delta F/F$ peak amplitude divided by the mean $\Delta F/F$ of 15 frames prior to stimulation) are shown in Scatter Plots with single datapoints. $\Delta F/F$ for single traces as well as global means per genotype are visually represented via heatmaps.

Data acquisition as well as image processing were performed blinded.

3.4 Behavioral assays

3.4.1 Mechanical nociception assay

Special attention was paid to precise staging of larvae like mentioned in (Hoyer et al., 2018). Therefore approximately 25 virgins and 10 males were collected and mated for one day. Followed by timed egg deposition for 3 – 6 h at 25 °C. After this timespan, approximately 100 – 150 embryos should be observed in vials to be used. At 96 (± 3) h AEL all larvae should be 3rd instar foraging stage and not yet leaving the food.

Mechanical nociception assays were performed related to (Zhong et al., 2010), with minor modifications. Larvae were washed and placed on a sylgard (SylGard 182 Silicone Elastomer Kit; Dow Corning) filled petridish (Ø 10 cm) and slightly covered with water. Each larva was stimulated with a self-made, 40 mN calibrated, Von-Frey-filament. "Caperlan Line Resist" fishing line (4.11 kg tractive force, Ø 0.22 mm) was cut to a length of 20 mm and attached in 90° angle to a plastic stick such that ~ 15 mm of the filament protruded from the end of the stick (Figure 12A). The force of the fiber was calibrated pressing it to a balance until the fishing line was bent and thus maximal force was applied. Weight was recorded and converted to force by multiplying the measured grams by a factor of 9,81 m/s2 (Figure 12B - C). The filament was shortened till a force of 40 mN was accomplished. Each stimulator was calibrated 10 times.
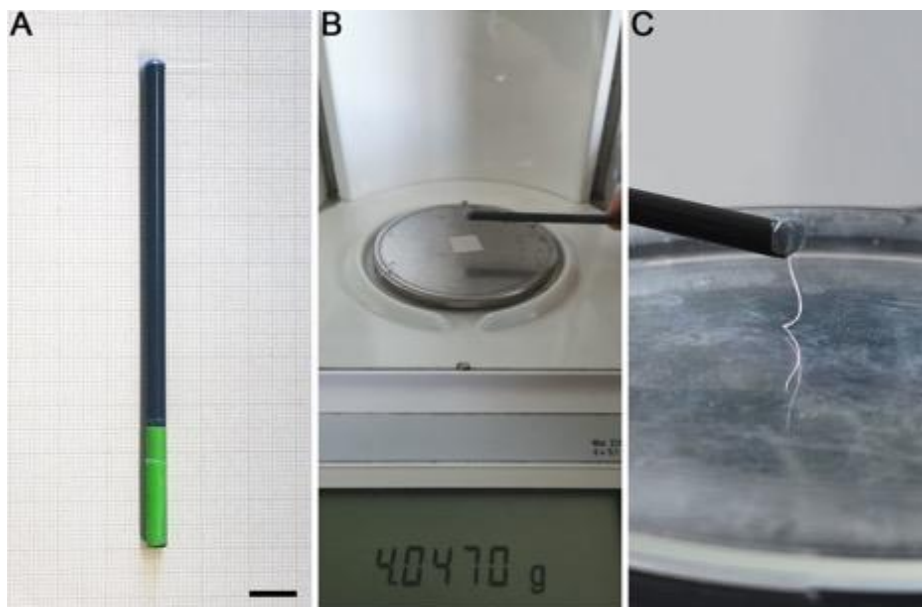

Figure 12. Von-Frey-filament for mechanical nociception assay. (A) Self-made Filament for mechanical stimulation. Scale bar: 1 cm. **(B)** Calibration on a scale to ~ 40 mN. **(C)** Maximal force application is reached when filament is pressed in 90 ° angle to surface and fiber bends.

Noxious mechanical stimuli were delivered by rapidly depressing the larva with the filament on the dorsal side (abdominal segments A5 to A8) (Figure 13A). The stimulus was delivered and released as quickly as possible. The quick release allows the larvae to perform escape locomotion behavior. A positive nociceptive response was scored if at least one nocifensive characteristic "corkscrew-like roll" (rotation around the anterior/posterior axis) occurred after the mechanical stimulus (Figure 13B). Each larva was tested only once. All datasets were generated from at least 5 independent trials each representing 20 – 30 larvae. Only normal behaving larvae – exhibit crawling/searching behavior before and rolling or crawling behavior after mechanical stimulation – where tested and counted.
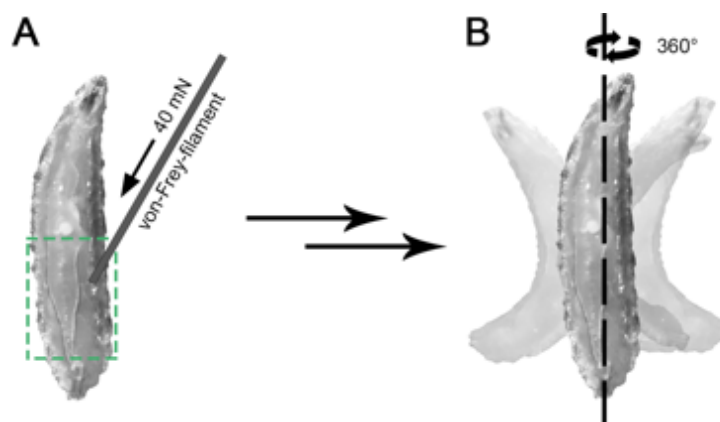
Figure 13. Schematic illustration of mechanical nociception assay. (A) Scheme shows appropriate region for mechanical stimulation with a 40 mN calibrated von-Frey-filament between A5 to A8 hemisegment of 3rd instar larvae. **(B)** Montage of C-shaped bending behavior prior to characteristic nocifensive "corkscrew-like roll" (360 ° rotation around the A/P axis).

3.4.2 Optogenetic nociception assay

The optogenetic nociception assays were performed similar to the mechanical nociception assay described previously (compare chapter 3.4.1). 3_{rd} instar larvae for optogenetic experiments, were placed in a 200 µl waterdrop on a petri dish (Ø 10 cm, bottom covered with sylgard) and monitored under a fluorescent microscope (Olympus 8ZX16). In each set of experiments, three larvae were analyzed simultaneously. Larvae were illuminated for 180 seconds (475 nm, 198 µW/mm2). After the light-protocol was finished, noxious mechanical touch assay was performed like previously described. For all optogenetic behavior assays each 3_{rd} instar larva was stimulated only once.

3 Materials and Methods

3.5 Drug induced neuropathy assay

Staged vials were observed till at least 90 % first instar larvae have emerged (~ 24 – 30 h AEL) prior drug application. Paclitaxel (Taxol; S1150 Absource Diagnostics) or an equivalent amount of vehicle (Dimethyl sulfoxide, DMSO; W387520 Sigma Aldrich) was applied to the food and gently mixed in. The amount of substance was calculated for an end concentration of 10 – 40 μM accordingly. At 96 – 120 (± 3) h AEL all larvae should be 3rd instar foraging stage and not yet leaving the food. Behavioral assays were than performed like described previously (compare chapter 3.4.1).

3.6 Statistical data analysis

Data were analyzed in Prism 7 or 8 (GraphPad Software, La Jolla, USA). Statistical tests were used as indicated in figures or corresponding data tables. Data are reported as mean ± SEM, n indicates the sample number and p denotes the level of significance (*p ≤ 0.05, **p ≤ 0.01, ***p ≤ 0.001).

4 Results

4.1 Functional characterization of dCirl in nociceptors

After dCirl expression and its function in lch5 chordotonal organs (type I sensory neurons) was described by Scholz and co-workers, basal work to unscramble the role of dCirl in *Drosophila* was done (Scholz et al., 2015, 2017). However, besides the involvement in gentle touch and vibration perception, we still lack information of mechanosensory properties dCirl may be involved. To this end, we focus on larval C4da sensory neurons and investigate molecular mechanisms of dCIRL activity using noxious mechanical stimuli in combination with optogenetic tools to manipulate second messenger pathways. In addition, we make use of a chemical induced neuropathy model to test for an involvement of aGPCR signaling in the malfunctioning PNS.

4.1.1 Cirl is expressed in larval nociceptors

While previous studies only focused on investigating *dCirl* function in ChO (Scholz et al., 2015), a transcriptional driver of dCirl (*dCirlGAL4*) used in this work, also demonstrated dCirl expression in md sensory neurons.

Interestingly, a subtype (type II class IV) of these md neurons are essential for perception of noxious mechanical stimuli (compare chapter 1.1.2.2). To answer the question if dCirl is expressed in these mechanosensitive C4da neurons, co-expression-analysis were performed.

As shown in Figure 14, higher magnification displayed dCIRL in lch5 chordotonal organs – recognizable due to their prominent five mono-scolopidial shape, like described recently (Scholz et al., 2015) – as well as co-localization between dCirl promotor driven CD4-tdTomato (membrane targeting sequence CD4 fused with tandem dimer fluorescent tag for increased brightness (Han et al., 2011)) and ppk-CD4-tdGFP the marker which was used to outline C4da sensory neurons in the PNS. Indeed we did observe that ppk-positive cells also expressed *dCirl*. This was verified by double fluorescence labeling

using *ppk-CD4-tdGFP* and *dCirlGAL4* that drives the expression of a nucleus targeted *UAS-RFPnls* (Figure 14 Bottom). Cell bodies of lch5 neurons (positive control) as well as nuclei of C4da neurons showed RFP signals.

Based on this findings, first evidence for an involvement of CIRL in nocifensive mechanosensation was given.
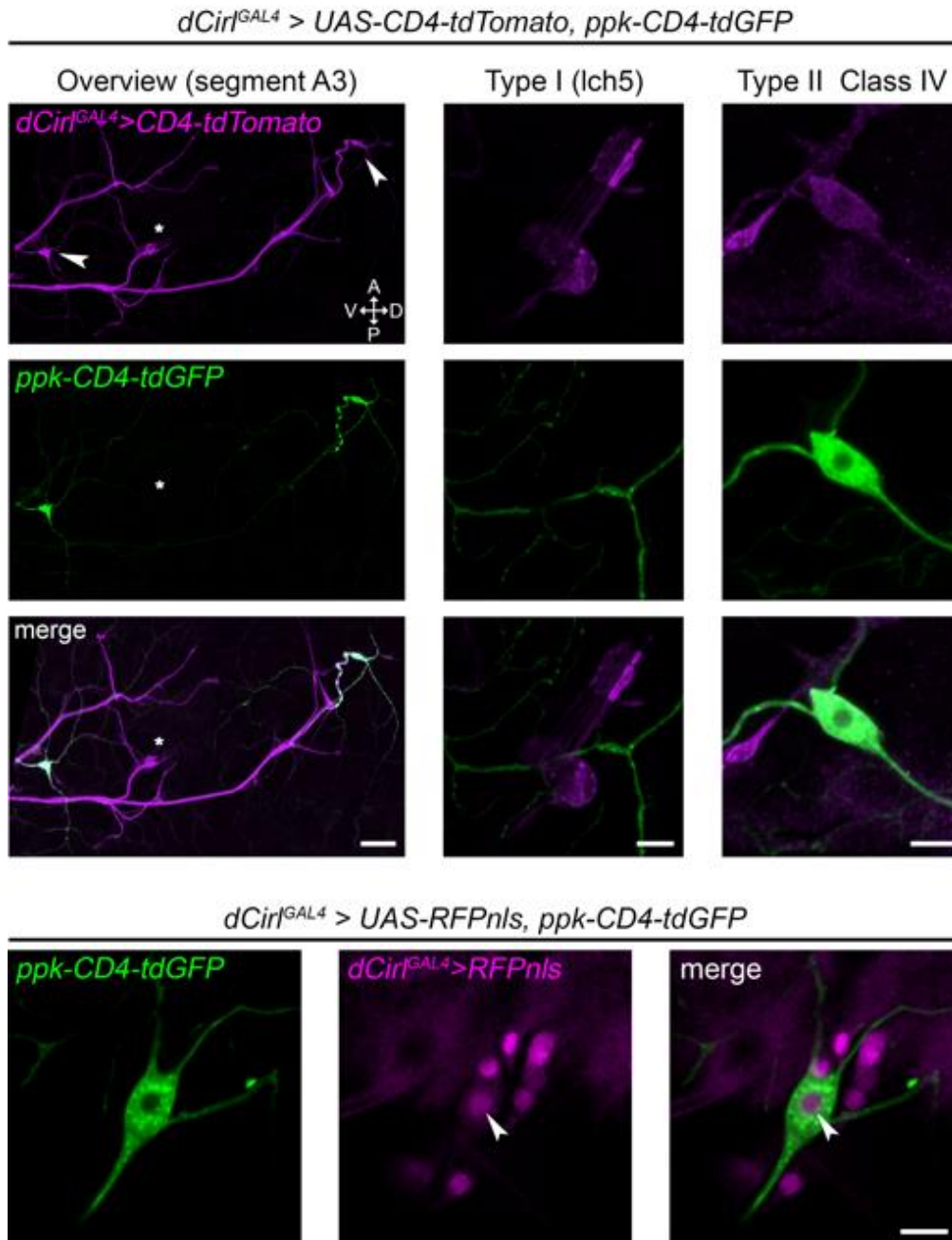
Figure 14. Cirl is expressed in larval type II class IV nociceptors. (Top) Expression pattern of dCirl promotor driven CD4-tdTomato and co-labelled C4da neurons (*ppk-CD4-tdGFP*) representatively shown in confocal images of abdominal hemisegment A3 (overview). Arrowheads indicate C4da cell bodies while type I lch5 neurons are marked by an asterisk. Scale bars: 50 µm for overview; 10 µm for details. (Bottom) Double labeling using ppk-CD4-tdGFP (green) and dCirlGAL4 driven UAS-RFPnls (magenta). Arrowhead indicate C4da cell nucleus. Scale bar: 10 µm.

4.1.2 Cirl shapes nocifensive behavior

Following immunofluorescence observations, a behavioral readout for harsh touch sensation was established like described previously (compare chapter 3.4.1) (Zhong et al., 2010). First, a dynamic range of behavioral responses had to be defined for wildtype animals that any kind of change, a more or less nocifensive reaction respectively, could be perceived. Forces between 20 and 50 mN were applied and approximately half of the tested wildtype larvae (53.22 % ± 1.13) responded with a stereotypic corkscrew like roll due to a mechanical stimulus of 40 mN with a calibrated von-Frey-filament (Figure 15A; Suppl. Table 1). This force was then used for the following experiments

After the behavioral readout was settled, the *in vivo* tests revealed significantly increased nocifensive response in *dCirl$_{KO}$* (75.37 % ± 2.68) (clean protein null allele created via ends-out targeting and homologous recombination from (Scholz et al., 2015)) compared to *dCirl$_{Rescue}$* (53.34 % ± 1.46) (rescued by re-insertion of wild-type dCirl sequences in *dCirl$_{KO}$* locus by (Scholz et al., 2015)) (Figure 15C). Not only was the nocifensive response increased, the mutant animals also displayed longer and more 360° rolls compared to the control group (data not quantified).

Since the mutant flies exhibit a ubiquitous null allele of CIRL, RNAi experiments were performed in order to resolve a cell specific effect of CIRL in C4da sensory neurons. While control animals show normal nocifensive response to noxious touch (*ppk$_{GAL4}$/+*: 50.14 % ± 3.97; *dCirl$_{RNAi}$/+*: 54.23 % ± 3.28), cell specific knockdown of CIRL in C4da neurons showed significantly increased nocifensive behavior (68.08 % ± 2.05) (Figure 15C). This data provides strong evidence, that dCirl shapes nocifensive behavior *in vivo*.

As autoproteolysis via the GAIN domain (chapter 1.3.2) seems to be a key mechanism of GPCR function, proteolysis deficient mutants (Scholz et al., 2017) were employed to check for phenotypes in the context of this paradigm, too. In contrast to the findings in the larval chordotonal organs by Scholz and co-workers (Scholz et al., 2017), *dCirl$_{T>A}$* mutants (abolished autoproteolytic activity as well as altered *Stachel* sequence (Figure 15B)) displayed wildtype responses (55.00 % ± 2.27), however, *dCirl$_{H>A}$* mutants delivered a knockout phenotype with significantly increased behavioral responses (73.78 % ± 1.85) (Figure 15C). Proteolysis deficient constructs were validated via PCR and sequencing, respectively (data not shown). This demonstrates that CIRL function *in vivo* is not dependent on CTF-NTF autoproteolysis function, a proper function of tethered

agonist *Stachel* seems to be dispensable but presumably an unmodified N-terminal fragment is obligate.

In addition, cell-specific rescue of behavior was successfully performed via expression of a *20xUAS-dCirl_{Flag}* (henceforth termed *UAS-dCirl*) transgene driven by *ppk-GAL4* driver (C4da sensory neurons) in the *dCirl_{KO}* mutant background (*dCirl_{Rescue}* /+ , *ppk_{GAL4}* /+: 53.70 % ± 3.20; *dCirl_{KO}, ppk_{GAL4}* / +: 75.30 % ± 2.20; *dCirl_{KO}, ppk_{GAL4}* / *UAS-dCirl*: 45.7 % ± 3.60) (Figure 15C). It must be pointed out that the Flag-tag, attached to the *UAS-dCirl* construct, has no varying effect on transgenic functionality in physiological processes (Scholz et al., 2015). Overexpression (OE) of dCIRL (via the *UAS-dCirl* transgene) exclusively in C4da neurons led to significantly reduced nocifensive response (37.01 % ± 2.80) which is even more pronounced in larvae raised at 29 °C (28.70 % ± 3.10) (due to the temperature dependence of the UAS/GAL4 system activity (Duffy, 2002)). However, OE at 29 °C induced a hypoalgesia-like condition in *Drosophila* larvae whereby a noxious stimulus provoke less nocifensive response compared to control animals (Figure 15C).

Notably this robust behavioral readout is characterized by its high reproducibility clearly represented through constantly reproducible values of nocifensive responses of control animals. Complete table of dataset including all results, sample size as well as statistically determined *P* values can be found in the supplement (Suppl. Table 2).

Taken together, dCIRL acts in a modulatory manner in mechanosensory neurons. In ChO, it was shown that dCIRL mediates mechanosensation in an up-regulatory manner upon vibration (Scholz et al., 2015, 2017), whereas it acts in a down-regulatory manner in type II class IV nociceptors.
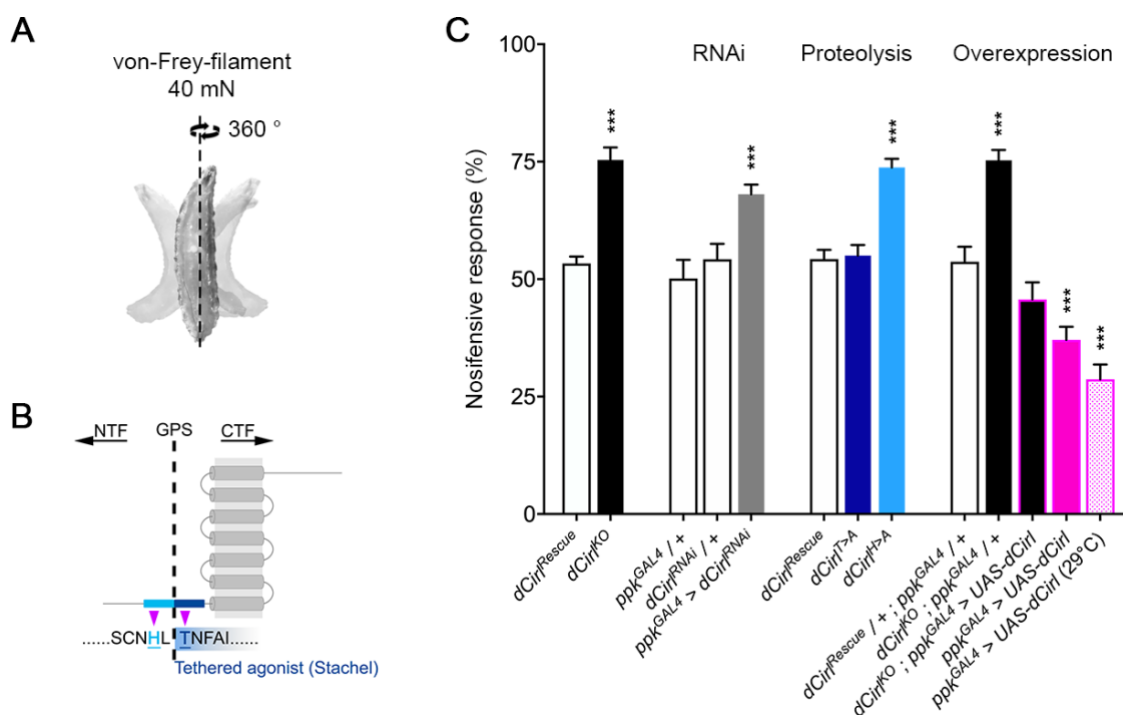
Figure 15. dCIRL shapes nocifensive behavior. (A) The mechanical nociception assay involves stimulation of *Drosophila* larvae with a calibrated von Frey filament (40 mN force), which induces a stereotypical behavioral response (360° cork-screw-like roll). **(B)** Graphical illustration of proteolysis- defective GPS variants of CIRL. The NTF is separated from CTF by the GPS in proteolyzable aGPCRs (Nieberler et al., 2016; Scholz et al., 2017). The C-terminal cleavage component hosts the tethered agonist (*Stachel*) sequence (light blue). Purple arrow: amino acids, necessary for GPS cleavage which were mutated in order to abolish autoproteolytic activity [data derived from (Scholz et al., 2017)]. **(C)** Quantification of nocifensive behavior in different genotypes. Increased nocifensive responses were observed in CIRL knockout mutant (*dCirl*KO), in nociceptor-specific expression of an RNAi construct (*dCirl*RNAi), as well as in the cleavage deficient *dCirl*H>A mutant. In contrast, expressing a *UAS-dCirl* transgene specifically in nociceptors (*ppk-GAL4*; C4da neurons), leads to reduced nocifensive responses. Data are presented as mean ± SEM. Asterisks denote the level of significance.

4.1.3 Nociceptor morphology of Cirl mutants

Following behavioral analyses, the morphology of *dCirl*KO flies was investigated. By doing so, the question whether behavioral changes arise from morphological changes due to knockout of dCIRL should be answered (Figure 16).

In order to reveal potential morphological defects of C4da sensory neurons in *dCirl*KO animals, 3rd instar larvae were examined via confocal live imaging. C4da neurons were visualized by *ppk-GAL4* driven *UAS-CD4-tdTomato* expression in control and knockout flies respectively (Figure 16A). Quantification of total dendritic length revealed no

significant change, however, numbers of terminals showed a mild reduction in mutant flies (Figure 16B,C; Suppl. Table 3-4).

To uncover dendritic complexity in more detail, numbers of dendritic intersections in relation to increasing distance from cell somata where measured employing Sholl-analysis (Sholl, 1953) (Figure 16D, E). It turned out that dendrites distal from the cell bodies are slightly less branched in *dCirl*KO compared to control neurons (Figure 16F). This effect might cause the slight decline in numbers of terminals in knockout flies.
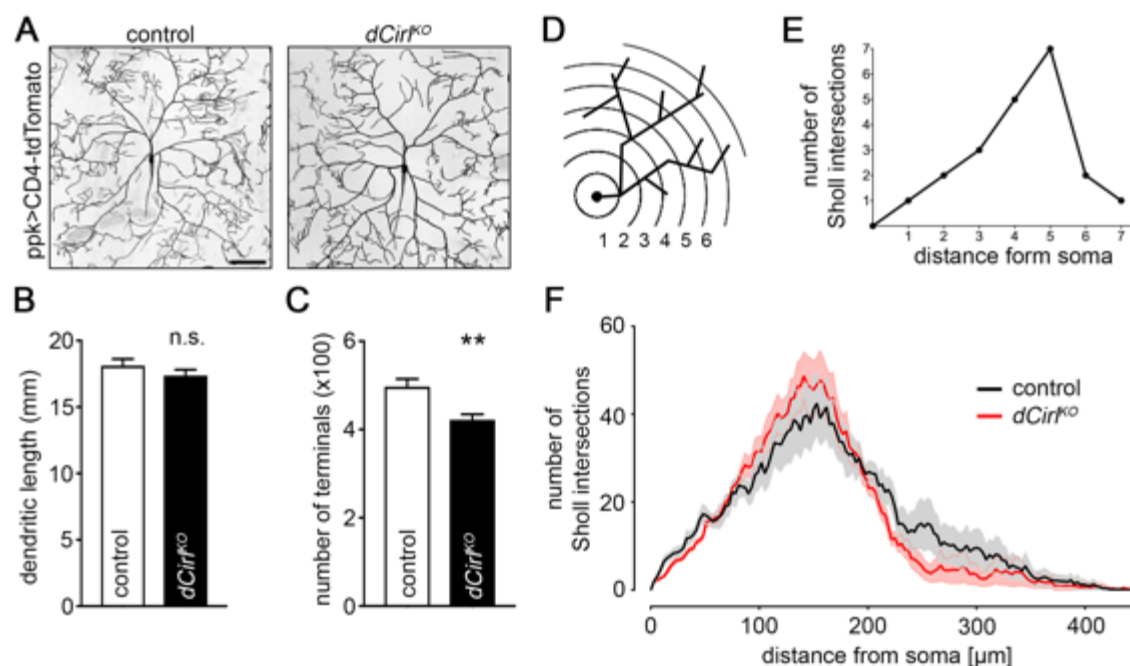
Figure 16. Morphology of C4da neurons of CIRL mutants. (A) Representative images of C4da neurons (*ppkGAL4 > UAS-CD4-tdTomato*) of control and *dCirl*KO mutant animals respectively (image acquisition by Chun Hu, ZMNH). **(B)** Quantification of dendritic length as well as numbers of dendritic terminals **(C)**. **(D, E)** Schematic explanation of Sholl analysis. Equidistant concentric circles are placed around the soma of a cell of interest and counted intersections are plotted against increasing distance from center. **(F)** Sholl analysis of *dCirl*KO and control neurons display slightly reduced high order branches compared to control which explains the mildly reduced numbers of terminals, respectively. Data are presented as mean ± SEM. Asterisks denote the level of significance. Scale bar: 100 μm.

4.2 Potentiation of nociceptor function by cAMP

With the description of a genetically encoded photoactivated adenylyl cyclase bPAC by Stierl and coworkers, a tool to optogenetically modify second messenger pathway through elevation of cAMP (cyclic adenosine monophosphate) levels has been made available to the scientific community (Stierl et al., 2011). In light of the recent project, bPAC was already successfully employed to manipulate cAMP levels within the *Drosophila* lch5 ChO. Here, it could be shown that a rise of intracellular cAMP concentrations by optogenetic, decreased mechanosensitivity of ChO neurons and FRET measurements demonstrated that dCIRL normally transduce mechanical stimuli into a decline of cAMP levels (Scholz et al., 2017).

Manipulation of intracellular cAMP levels in vivo were performed by optogenetics and hypomorphic phosphodiesterase (PDE) mutations, combined with the previous introduced behavioral readout for quantification of nocifensive behavior.

To uncover intracellular signaling by dCIRL in nociception, bPAC was expressed cell-specifically in C4da neurons using the *ppk-GAL4* driver, thus cAMP levels could be increased upon photo stimulation with blue light (475 nm) (Figure 17A).

While wildtype animals showed no detectable differences in nocifensive response behavior during blue light illumination, the undriven bPAC construct showed slight dark activity. This is recognizable by spontaneous bending – a pre-stage of the stereotypic corkscrew-like roll – during light stimulation as well as in the dark control. In contrast, stimulated and spontaneous nocifensive responses can be promoted and elicited upon bPAC activation in C4da neurons. These observations are even more pronounced in *dCirl$_{KO}$* background (Figure 17B). Noticeably, while the amount of mechanical stimulated rolling occurs comparably among tested groups, spontaneous rolling was observed approximately three times more in *dCirl$_{KO}$* background compared to *ppk$_{GAL}$ > UAS-bPAC* flies.

Taken together, these results suggest that photoinduced cAMP elevation in wildtype C4da neurons stimulates neuronal activity resulting in behavioral responses observed in *dCirl$_{KO}$* mutants, while bPAC activation in the *dCirl$_{KO}$* background even further encourage nociceptors.

To further validate the findings from optogenetic experiments, flies with specific PDE mutations were tested. The *dunce1* and *dunceML* mutants are hypomorphic alleles with lower PDE activity. They hydrolyze cAMP at a significantly slower rate compared to wildtype and are therefore less efficient in generating a cAMP signal. The dunce mutants have remaining cAMP hydrolysis rates of ~ 73 % (*dunce1*) and ~ 34 % (*dunceML*) (Davis et al., 1981).

It becomes apparent that both these mutants show significantly increased nocifensive behavior to noxious stimuli of 40 mN (Figure 17C, Suppl. Table 5). It is not surprising that between the mutants themselves there is statistical significance in the nocifensive behavior considering their difference in cAMP hydrolysis rates. With this observation, we strengthen the outcome from optogenetic experiments achieved previously.

Thus, CIRL is hypothesized to modulate nozizeptor activity by decreasing cAMP levels due to the fact that increased intracellular cAMP levels result in behavioral knockout phenocopy.
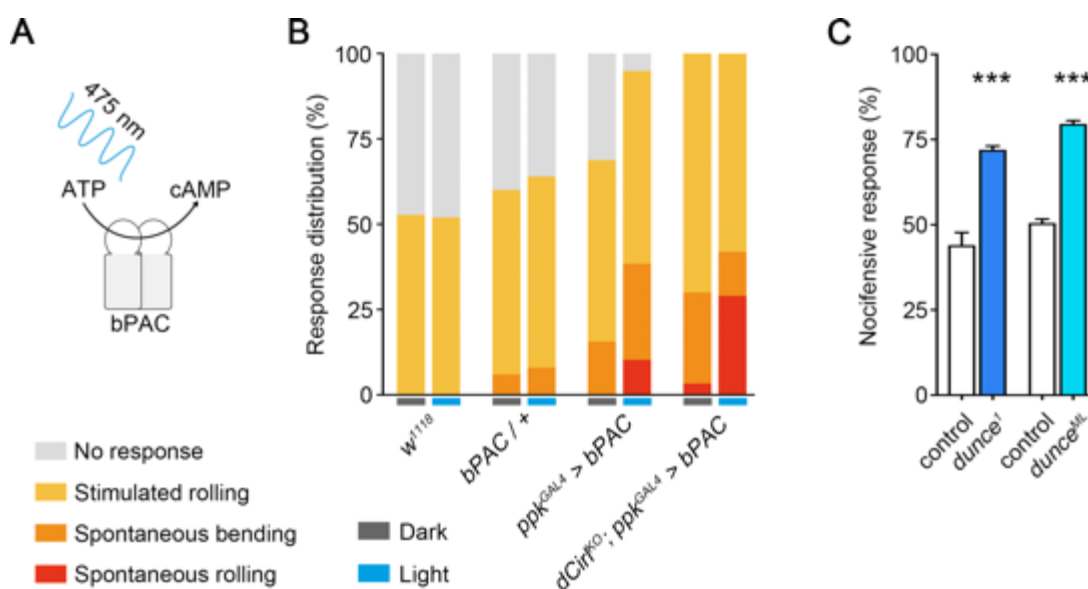
Figure 17. Potentiation of nociceptor function by cAMP. (A) Schematic illustration of cAMP production by the blue light-activated adenylyl cyclase (bPAC). **(B)** Optogenetic assay. Stimulated and spontaneous nocifensive response can be promoted and elicited, respectively, upon bPAC activation in C4da neurons (blue labels: photo stimulation; black label: dark control). Larval behavior was observed during 120 s illumination (475 nm) and after mechanical stimulation (40 mN). **(C)** Hypomorphic PDE mutants exhibit increased nocifensive response. Analysis of PDE mutants with remaining cAMP hydrolysis rates of 73 % (*dunce1*) and 34 % (*dunceML*) compared to their control (Davis et al., 1981), respectively, show significant increased nocifensive behavior while a statistical relevant effect within PDE mutants is negligible. Data are presented as mean ± SEM. Asterisks denote the level of significance.

4.3 Functional imaging of peripheral nociceptors

The results presented above suggest that dCIRL is important for perception (sensing mechanical cues by specific neurons) and/or processing (by neurons in the ventral nerve cord) of noxious mechanical stimuli. This is indicated by increased nocifensive response behavior in larvae lacking dCIRL.

Hence, to differentiate both processes and the involvement of dCIRL in these, we analyzed C4da sensory neurons in the PNS employing live calcium imaging during mechanical stimulation. To do so, the genetically encoded calcium indicator GCaMP was combined with a mechanical stimulation protocol to investigate calcium responses in subcuticular C4da neurons *in vivo*. GCaMPs consists of circularly permuted green fluorescent protein (cpGFP) inserted between calmodulin (CaM) and an M13 peptide (from myosin light chain kinase). Upon calcium binding, conformational changes in the CaM–M13 complex induce fluorescence changes. CaM binds the M13 in the presence of Ca_{2+}, this coupling reverses when Ca_{2+} is absent (Figure 18A) (Broussard et al., 2014).

Larval handling and imaging were performed as described previously (compare chapter 3.3). In short: filleted larva are flipped 180° such that the cuticula is facing upwards. Mechanical stimulation is applied via a sealed glass electrode (tip ø 20 µm) which executes tissue displacement of 100 µm in 90° angle downwards (Figure 18B). Fluorescent changes due to calcium changes are acquired meanwhile. Low intensity fluorescence (515 nm) can be observed prior to stimulation. Application of a mechanical stimuli will cause Ca_{2+} influx/release in the neuron, resulting in changed fluorescence levels over time (Figure 18C).
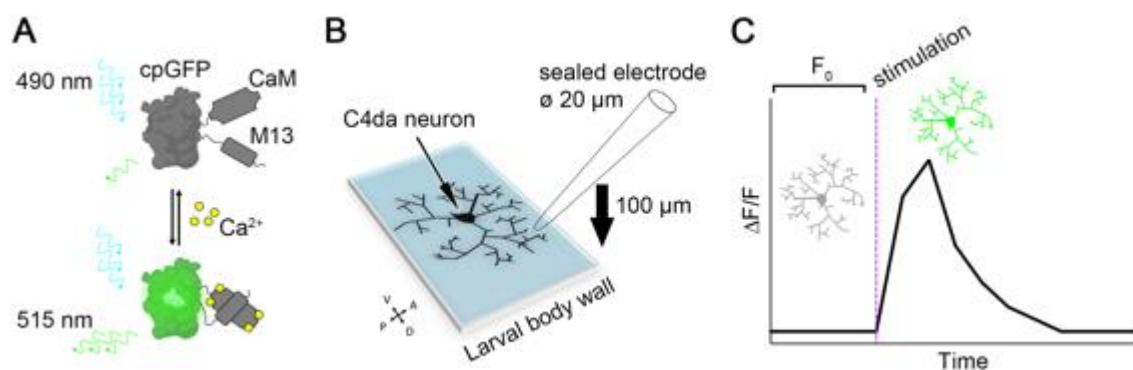
Figure 18. Principle of functional calcium imaging measurements. (A) schematic structure of the Ca2+ indicator GCaMP which changes its conformation and fluorescence property upon binding of Ca2+. **(B)** Mechanical stimulation of C4da sensory neurons via a sealed glass electrode with tip diameter of 20 μm causing tissue displacement of 100 μm in 90° angle. **(C)** Schematic illustration of evoked calcium signal in relation of time, whereby ΔF/F increases by increasing GCaMP fluorescence in the presence of Ca2+.

Calcium imaging measurements of C4da neurons of *dCirlKO* and control animals showed a rapid increase in intracellular calcium in knockout larvae and declined approximately one second after stimulation ends (Figure 19A), whereas controls react only minor upon mechanical stimulation. This is already visible in single traces of controls and knockout respectively (Figure 19A', A''). In *dCirl* mutants, the peak calcium response (measured at the cell soma of ppk-Gal4 expressing neurons) was significantly increased relative to wildtypes (Figure 19B, Suppl. Table 7). The peak-amplitude-quotient (maximal ΔF/F peak amplitude divided by the mean ΔF/F of 15 frames prior to stimulation) revealed that stimulated relative peak-amplitudes in *dCirlKO* is approximately 115.5 times higher than their corresponding baseline fluorescence while in controls peaks are approximately 42.2 times increased (Figure 19C, Suppl. Table 8).

Thus, these results suggest that the hypersensitive behavioral responses to noxious touch observed in *dCirlKO* animals (see chapter 4.1.2) are indeed a consequence of hypersensitive force sensitivity in C4da neurons.
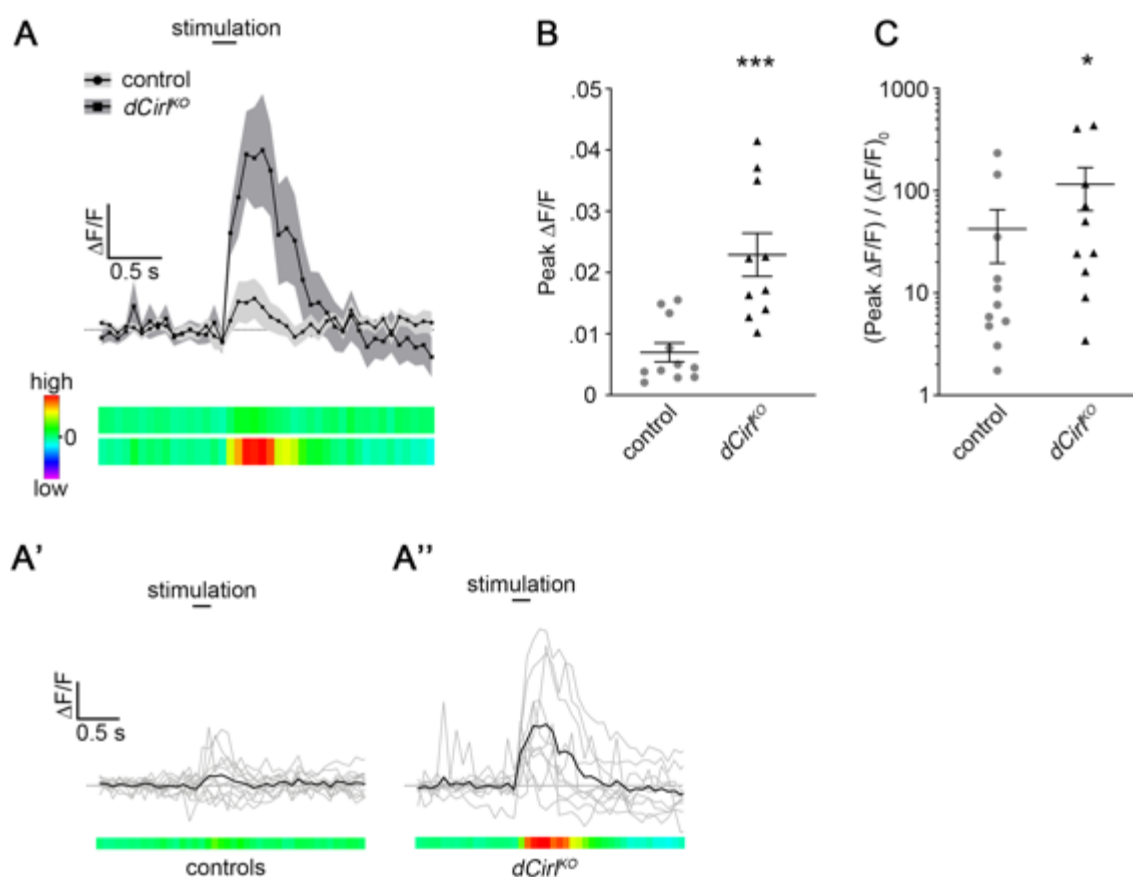
Figure 19. Enhanced force-triggered Ca$_{2+}$-responses of C4da neurons. (A) Top: Traces showing average ΔF/F of C4da neurons before, during, and after mechanical stimulation in controls and *dCirlκo* larvae respectively. Dotted line indicates baseline. Scale bar: 0.005 ΔF/F; 500 ms. Bottom: Heatmaps represent the average response data, with ΔF/F values represented by the color scale (far left). **(A', A'')** Overlaid single traces of Ca$_{2+}$-responses to mechanical stimulation, related to **(A)**. Each grey colored trace represents an individual stimulus. Average response to stimulation is shown in black trace. Each cell is stimulated just once during measurement. Scale bar: 0.01 ΔF/F; 500 ms single representative traces of each genotype are given below. **(B)** Average peak ΔF/F of C4da neurons in response to stimulation of each genotype displays significantly increased amplitude of *dCirlκo* cells. Also present in the peak-amplitude-quotient (maximal ΔF/F peak amplitude divided by the mean ΔF/F of 15 frames prior to stimulation) where stimulated peak-amplitudes in *dCirlκo* are ~ 2.7 times higher as against controls **(C)**. Data are presented as mean ± SEM. Peak analysis are shown in Scatter Plots with single datapoints. ΔF/F for single traces as well as global means per genotype are visually represented via heatmaps; purple to red representing low to high ΔF/F. Asterisks denote the level of significance.

4.4 Cirl in Taxol mediated neuropathy

A second subproject of this thesis was to establish a peripheral neuropathy model induced via drug application. In collaboration with Heike Rittner "Center for Interdisciplinary Pain Medicine – University Hospital Würzburg", drug IPN in *Drosophila* was elicited using Taxol (Paclitaxel). This will facilitate that potential findings can later be transferred to neuropathy models in rodents and patients.

By combining our robust behavioral paradigm with morphological analysis, we shed light on the influence of dCIRL in the progression of pathology following the Taxol IPN in *Drosophila* larvae.

4.4.1 Introducing a neuropathy model

We first set a paradigm for drug application to larval *Drosophila in vivo*. Taxol was applied 24 h AEL after embryos emerged to early first instar larvae, in order to avoid developmental interferences (neurogenesis as well as axon pathfinding are completed till then (Prokop, 1999)). Morphology and behavior were assessed 96 - 120 (± 3) h AEL when all larvae should be 3rd instar foraging stage and not yet leaving the food (Figure 20A). Taxol was employed in different concentrations (10, 20 and 40 µM) and initial experiments showed that all animals treated with the drug, irrespective of used concentration, showed very strong nocifensive behavior in the presence of mechanical stimulation (Figure 20B, Suppl. Table 9). Additionally, larvae developed ~ 24 h slower resulting in latest 120 h AEL till they reached 3rd instar stage. Whereas in DMSO (vehicle) treated control animals no changes in behavioral responses occurred, a decrease in developmental speed was observed.

Necrotic patterns as pathological effect of Taxol treatment in higher concentrations (20 µM and more) are constituted frequently (Figure 20C', C''). Morphological analysis using confocal microscopy revealed dendritic degeneration in type II class IV sensory neurons (labelled by *ppk-CD4-tdGFP*) when larvae develop in the presence of 10 µM Taxol. An intermediate phenotype of fragmentation (Taxol mild) can be observed as well as a more severe form of peripheral neuropathy (Taxol severe) (Figure 20D). Furthermore, fragmentation and swellings of axons and dendrites in the complete larval

PNS are apparent (Figure 20E', E'') which is comparable to findings from the DiAntonio lab (Bhattacharya et al., 2012).
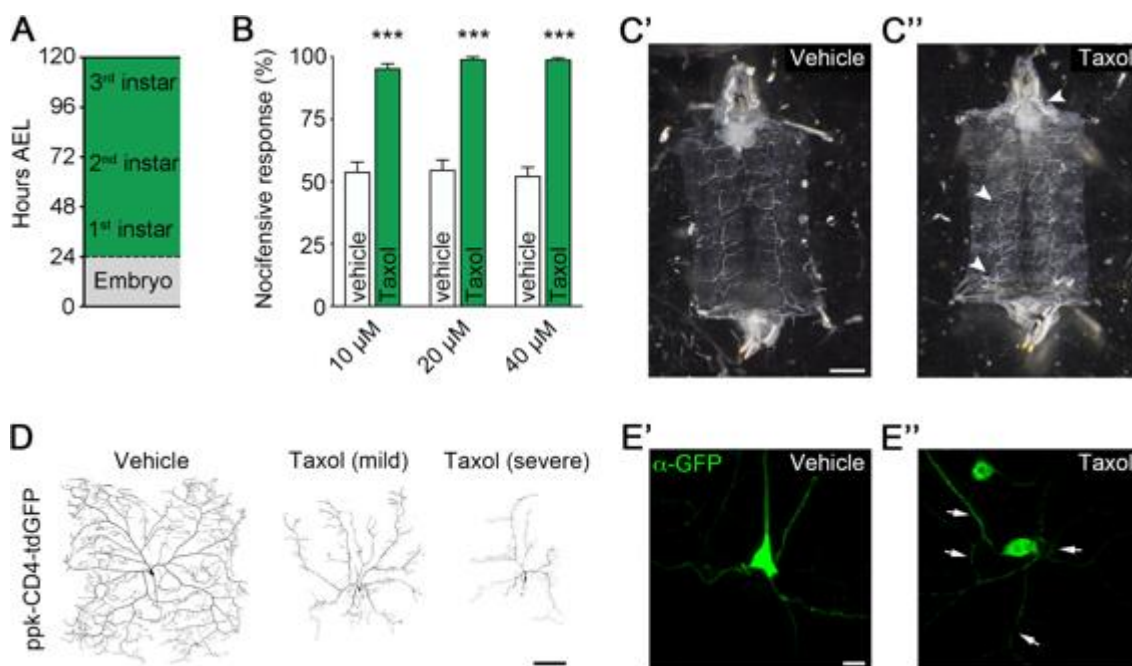
Figure 20. Taxol induces peripheral neuropathy model in *Drosophila* larva. (A) Timetable for Taxol application and behavioral experiments. Drug application was carried out 24 h AEL. **(B)** Nociception assay in the presence of Taxol revealed significant increased nocifensive behavior irrespective of deployed Taxol concentration whereas vehicle treated animals show no peculiarities. Concentrations of 10, 20 and 40 µM Taxol were tested as well as corresponding amount auf vehicle. **(C', C'')** Dark necrotic patterns can be observed in larval preparations upon Taxol treatments of higher concentrations (> 20 mM) (arrowheads). **(D)** Neuronal degeneration in C4da neurons (labelled by *ppk-CD4-tdGFP*) is observable when larvae develop in the presence of 10 µM Taxol. Intermediate phenotype of fragmentation (Taxol mild) can be observed as well as a more severe pattern (Taxol severe). **(E', E'')** Immunohistochemistry revealed fragmentation and swellings of dendrites (arrows) of C4da cells. Scale bar, (C' ,C'') 500 µm, (D) 100 µm, (E) 10 µm. Data are presented as mean ± SEM. Asterisks denote the level of significance.

4.4.2 Influence of Cirl on Taxol-induced phenotypes

Next, we examined the influence of CIRL in the context of the established Taxol IPN model. It became apparent, that in *dCirl*$_{KO}$ background, the nocifensive behavior of Taxol treated animals is significantly increased and indistinguishable from WT animals treated with Taxol (Figure 21A). Vehicle treated animals, however, showed comparable results to previous findings (compare 4.1.2).

Based on the results that cell specific OE of CIRL in C4da neurons had reduced nocifensive response significantly, we applied OE experiments in the IPN model. We found that CIRL OE led to the expected reduction of behavioral responses in vehicle treated, but also to a huge reduction of nocifensive behavior (declined by ~50 % compared to WT + Taxol) in Taxol treated larvae. The toxic effect of Taxol is still present in OE group indicated by a slightly increased nocifensive response (OE + vehicle: 37.12 % ± 2.78; OE + Taxol: 46.34 % ± 2.37) (Figure 21A; Suppl. Table 10).

Having set out behavioral experiments, we checked for underlying morphological changes that might cause the behavioral phenotypes. To answer that, morphological analysis were performed to reveal the influence of dCIRL in progression of pathology following the Taxol IPN in *Drosophila* larvae (Figure 21B - F). Quantitative observations of C4da sensory neurons unveil that Taxol treatment results in both dramatically reduced total dendrite length, as well as number of terminals (Figure 21B, C; Suppl. Table 11-11). This is consistent with previous work (Bhattacharya et al., 2012).

Interestingly, the same parameters are already significantly reduced in untreated *dCirl* OE larvae. Taxol application results in inhomogeneity of datapoints with significant reduced dendritic length and a slight, but not significant reduction of terminal numbers.

To analyze dendritic complexity in more detail, Sholl analysis was carried out (Figure 21D). In comparison to controls, *dCirl* OE in C4da neurons demonstrate reduced dendritic complexity mainly in proximal to medial parts of neurons (200 – 450 μm from soma). Whereas Taxol application causes strong reduction of Sholl intersections in WT larvae which is even more pronounced in *dCirl* OE. Comparison of the OE group revealed strong effects on the medial to distal part (200 – 450 μm) of the neurons. These results go along with previous analysis of total dendrite length as well as numbers of dendritic terminals (Figure 21B, C)

In addition to the Sholl analysis, reverse Strahler analysis was performed to survey possible changes of branch order in relation to absolute branch numbers (Figure 21E) (Strahler, 1952; Marasco et al., 2013; Ledderose et al., 2014). In C4da neurons, exposed to Taxol, the number of branches within the first branch orders was perceptibly reduced, whereas higher order branches seemed to be unaffected. In return, *dCirl* OE C4da neurons displayed an increased branch number of lower order dendrites compared to controls (Figure 21F). Furthermore, OE animals are lacking higher Strahler numbers (> 12) completely. In the presence of Taxol, again, branch order was drastically reduced overall.

However, a shift towards higher ordered branches was observed, indicating increased dendritic branching of remaining dendritic arbors.

Taken together, *dCirl* function was tested in a drug IPN model where it was shown that cell specific OE of *dCirl* rescues nocifensive behavior but not nociceptor morphology.
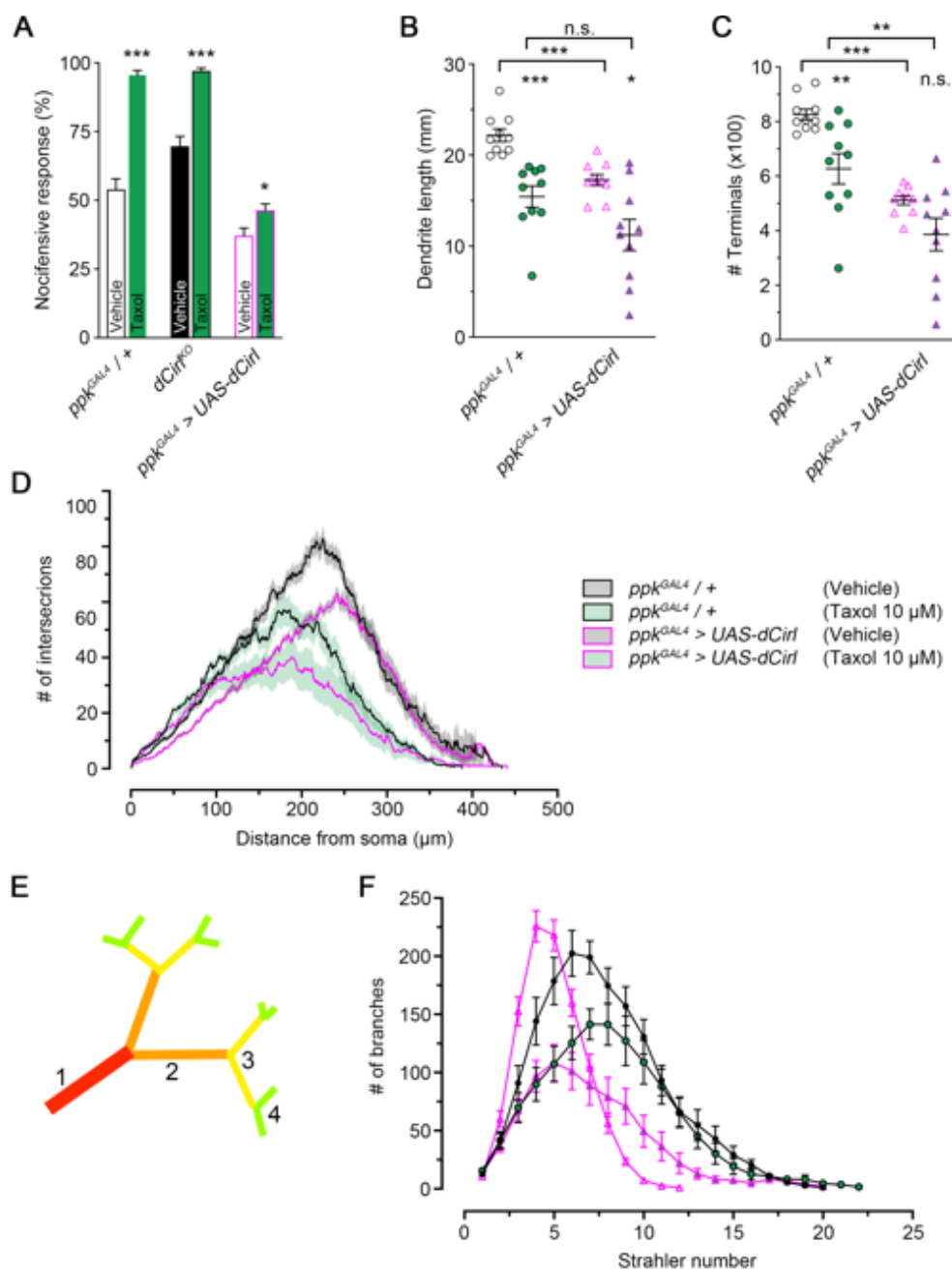
Figure 21. Influence of Cirl on Taxol-mediated behavioral and morphological phenotypes. **(A)** Behavior analysis of Cirl Phenotypes in a Taxol IPN model. **(B)** Quantitative analyze of total dendritic length and number of dendritic terminals **(C)**. **(D)** Sholl analysis was performed to quantitatively visualize C4da neuron complexity. **(E)** Schematic illustration of branch numbering in Strahler analysis. Number of dendrites are plotted against increasing branch order, beginning with the main branch and increased number for following arbors. **(F)** Strahler analysis of C4da neurons go along with previous findings. Data are presented as mean ± SEM. Asterisks denote the level of significance.

5 Discussion

For many decades, *Drosophila* has been one of the profitable organisms in finding and describing genes involved in various aspects and cause of diseases. Thereby the focus on clinically relevant physiological processes such as nociception and neuropathy, which are also the hallmarks of this thesis, strengthened *Drosophila* as a powerful tool in this field.

The aim of this study was, to reveal the function of the aGPCR dCirl in the context of noxious mechanosensation. Previous work demonstrated that CIRL is involved in mechanosensation perceived by the lch5 chordotonal organs (Scholz et al., 2015). *dCirlKO* larvae exhibit a diminished response to mechanical stimulation of lch5 pentascolopidial organs. Hence, we supposed that also mechanosensation of noxious stimuli may be altered.

Confocal fluorescence microscopy was used to answer the question if CIRL is expressed in C4da sensory neurons, the main neurons for perceiving noxious touch (Hwang et al., 2007). First trials to visualize CIRL via a chromophore fusion (*dCirlRFP*) and FLAG-tagged (*dCirlFLAG*) construct in the PNS of 3rd instar larvae were challenging/unfeasible. This might be the case because of the low endogenous expression levels of CIRL. This is similar to published data of other aGPCRs (e.g. LAT-1 in *C. elegans* or GPR126 in rodents) (Kobilka et al., 2007; Langenhan et al., 2009).

Likewise, our collaboration partners from the University Hospital Würzburg reported challenges in visualizing LAT1-3 in rodent dorsal root ganglions (unpublished data) which maybe also caused by low copy numbers expressed or also posttranslational modification (e.g. phosphorylation) may cause difficulties in visualization.

To bypass the issue of low expression, we used a GAL4 construct under control of the endogenous *dCirl* promotor to drive different fluorescent markers like *UAS-CD4-tdTomato* (Han et al., 2011) or *UAS-RFPnls* (nuclear-localized red fluorescent protein) and perform antibody based stainings in order to enhance visibility.

By doing so, we were able to visualize transcriptional activity of *dCirl* in the larval PNS especially in neurons like Type I sensory neurons (lch5) and Type II md neurons. These findings are comparable with published results of expression patterns of *dCirl* (Scholz et al., 2015). To check for *dCirl* transcription in nocifensive C4da neurons, we employed a cell specific fluorescent marker for type II class IV sensory neurons (*ppk-CD4-tdGFP*

(Han et al., 2011)). The results demonstrate that *dCirl* indeed is expressed in sensory neurons that are responsible for sensing noxious mechanical stimuli.

5.1 Cirl shapes mechanosensation in a modulatory manner

Based on the transcriptional activity of *dCirl* in type II class IV nociceptors, we employed a behavioral assay to investigate CIRL function in receiving noxious touch. Therefore, a very robust readout was used like described earlier (Tracey et al., 2003) and is the common standard in investigations of nocifensive behavior for years (Im et al., 2012; Kim et al., 2012; Milinkeviciute et al., 2012; Guo et al., 2014; Mauthner et al., 2014)

dCirl_{KO} mutant larvae exhibit a drastically increased nocifensive response behavior to noxious mechanical stimuli applied by a calibrated von-Frey-filament. To determine a cell-specific phenotype RNAi technique was used. By expressing *dCirl_{RNAi}* in C4da neurons via *ppk-GAL4* driver line, cell specificity was shown. Taken together, knockout and RNAi experiments display hyperalgesia-like behavior responses of *Drosophila* larvae, demonstrating that the aGPCR CIRL seems to be important for proper sensation of noxious touch stimuli by acting in a down-regulatory manner in nociceptors.

The hyperalgesia could be rescued by expression of a *UAS-dCirl* transgene in the knockout background. This is compatible to findings in lch5 neurons (Scholz et al., 2015).

Interestingly, OE of *dCirl* resulted in a hypoalgesia like behavior. This effect was even more pronounced under 29 °C condition where binary GAL4/UAS expression system works more efficient (Duffy, 2002). Thus, the right amount of aGPCR might be necessary for proper mechanosensation in nociceptors.

In addition, we tested autoproteolysis mutants of *dCirl*. All aGPCRs hold a juxtamembrane protein domain, the GAIN (GPCR autoproteolysis-inducing) domain, which acts as a autoproteolysis site in many aGPCR homologs (Liebscher et al., 2016; Nieberler et al., 2016).

Research on GAIN mediated GPS cleavage demonstrated that the proteolysis event play an important role in receptor function, membrane trafficking and receptor activation (Prömel et al., 2012; Nieberler et al., 2016).

Investigations of two CIRL autoproteolysis deficient mutants – $dCirl_{H>A}$ and $dCirl_{T>A}$, latter within the tethered agonist *Stachel* sequence – yield that the tethered agonist *Stachel* seems to be dispensable and larvae with disrupted NTF mutation showed knockout phenotypes. To verify these findings, mutants were confirmed using PCR and sequencing methods (data not shown).

Different models of aGPCR activation by the *Stachel* were described (Langenhan et al., 2013; Liebscher et al., 2013, 2014a, 2014b, 2016; Scholz et al., 2016) in which binding of a ligand or mechanical cues provoke conformational changes of the aGPCR N-terminus and thereby lead to the exposure of the *Stachel* and binding to the 7TM. This activation than is followed by initiation of second messenger pathways. The tethered agonist model of aGPCRs seems to be applicable for dCIRL function in mechanosensation of the lch5 chordotonal organ (Scholz et al., 2017).

We found that autoproteolysis is not necessary for proper function of dCIRL in C4da neurons but whereas the punctmutation within the NTF causes a knockout phenocopy, the punctmutation within the *Stachel* showed no conspicuity. Since the $dCirl_{T>A}$ mutation is located at the last residue of β-strand within the *Stachel*, I suppose that it is maybe not important for full activation of the receptor and causes no behavioral phenotype. However, $dCirl_{H>A}$ mutation phenotype might derive from a hampered receptor in which the *Stachel* cannot be liberated upon mechanical force. This hypothesis would fit to the described activation mechanisms of aGPCR by mechanical cues (Scholz et al., 2016).

It is also reported, that aGPCRs can mediate both *Stachel*-depended and *Stachel*-independent signaling by activating different pathways (Kishore et al., 2016; Purcell et al., 2018) which might be the case for CIRL as well and would explain our results, too.

Nevertheless, we were able to show, that Latrophilin/CIRL acts in a modulatory manner on mechanosensation. On the one hand *dCirl* mediates mechanosensation in an up-regulatory manner upon vibration in chordotonal organs (Scholz et al., 2015, 2016) and on the other hand it modulates nociception in a down-regulatory manner in C4da sensory neurons.

Behavioral analyses where followed by investigation of C4da morphology in *dCirlκo* background. The question should be answered, if behavioral effects, observed previously, are triggered through morphology alterations. Therefore, together witch the Soba lab in Hamburg, we investigated C4da neurons in more detail. Quantitative analyses revealed no changes in dendritic length and only mild effects in terminal numbers in *dCirlκo* mutants. This mild effect is due to faint reduction of distal branches compared to wildtype animals. These results show that behavioral changes are not caused by morphological changes, which is comparable to findings that structure of chordotonal organs appeared unaffected in *dCirlκo* mutants (Scholz et al., 2015).

To examine intracellular signaling by CIRL, the behavioral readout paradigm was combined with optogenetics. bPAC was used to create photoinduced cAMP elevation in wildtype C4da neurons. Thereby, stimulated and spontaneous nocifensive responses can be promoted and elicited to the level observed in *dCirlκo* mutants without bPAC expression. However, bPAC activation in *dCirlκo* background did even further increase nocifensive response to a maximal level where all larvae show nocifensive reaction, whether simulated or spontaneous.

These findings are supported by the analysis of hypomorph phosphodiesterase mutants (*dunce1* and *dunceML*) which have been, established for years, well characterized and frequently used in analyzing cAMP signaling cascades. These mutants hydrolyze cAMP at a significant slower rate than in wildtype (Davis et al., 1981; Maiellaro et al., 2016).

Thus, increased cAMP levels led to increased nocifensive response, indicating CIRL modulates neuronal activity by suppressing cAMP production.

In contrast to findings in *C. elegans*, where LAT1 interacts with G_s proteins and thereby elevate cAMP level (Müller et al., 2015), Scholz and coworker demonstrated G_i coupling of dCirl in *Drosophila* larval ChOs (Scholz et al., 2017).

So it was very astonishing that in ChO, *dCirlκo* as well as bPAC activation leads to disrupted mechanosensation by decline in neuronal activity. While in C4da sensory neurons we showed that *dCirlκo* led to an increased behavioral nocifensive response, so did bPAC activation as well. This results hypothesize that in both mechanosensing cell types dCIRL couple to G_i-protein pathway but the effector activity is oppositional.

All together strengthen the hypothesis that CIRL modulates mechanosensation in a highly cell and/ or species specific manner. In the feature, FRET measurements in combination

with pharmacological approaches could be applied, to reveal further details in cAMP signaling of larval nociceptors.

During the optogenetic assay, leak expression of the bPAC construct could be observed as well as high dark activity. Leak expression is constituted by altered response behavior in the undriven UAS-bPAC construct and dark activity – in ppk$_{GAL4}$>UAS-bPAC as well as in dCirl$_{KO}$ background larvae – is noticeable increased compared to controls without the bPAC construct. By employing the behavioral readout to new bPACs with enhanced light/dark ratio and less leak expression, a fast and reliable technic has been established to analyze those new optogenetic tools in a quantitative manner (unpublished data).

Findings from the behavioral assay suggest that perception and/ or processing of noxious mechanical stimuli is largely affected in larvae lacking CIRL. Hence, we analyzed C4da sensory neurons employing live calcium imaging during mechanical stimulation to ask the question, if neuronal activity in knockout animals maybe increased and thereby induce higher response. Wildtype C4da neurons showed only minor calcium responses upon mechanical stimulation, while cells of *dCirl$_{KO}$* background animals displayed force-induced calcium rise upon 100 µm touch displacement. These findings are similar to published results of rapidly increasing GCaMP signals in md neurons lacking the mechanosensitive K$_+$ channel SK (*small conductance calcium-activated potassium channel*) (Walcott et al., 2018). Thus, these results suggest that the hypersensitive behavioral response to noxious touch observed in *dCirl$_{KO}$* animals are indeed a consequence of hypersensitive force sensitivity in C4da neurons.

Recent findings from the Südhof lab showed that Latrophilin-3 mediates synapse formation in the hippocampus of rats by binding to FLRTs (fibronectin leucine-rich-repeat transmembrane proteins) and teneurins (Sando et al., 2019). Therefore, lacking Latrophilin-3 in hippocampal neurons cause hampered synaptic transmission represented by decreased spontaneous mEPSC frequency as well as declined evoked EPSC amplitude. Synaptic alteration due to loss of Latrophilin cannot be excluded in our experiments but I would suspect that an attenuated synaptic transmission would result in less behavioral response upon stimulation. Further experiments can include multitouch assays or drug application like SQ22536 to inhibit adenylyl cyclase activity and the analysis of resulting intracellular Ca$_{2+}$ responses upon these conditions. Also electrophysiological measurements can be applied to test for an involvement of dCIRL in synaptic transmission between nociceptors and downstream neurons.

Structural characteristics of CIRL imply a function in the molecular signaling cascade where it can act in a modulatory manner on molecules, transducing mechanical forces to intracellular signals. During the last few years, research in the field of mechanosensation advanced and major key players have been identified in *Drosophila* as well as rodent models. Thus, different potential targets or interaction partners of aGPCRs arose:

a) The DEG/ENaC channels, are usually Na_+ selective and were already shown to be necessary for noxious mechanosensation. Knockout experiments of *pickpocket* displayed highly reduced nocifensive response behavior upon mechanical stimulation (Zhong et al., 2010; Mauthner et al., 2014).

b) Piezo channels are laboratory-confirmed to play an important role in mechanical nociception in *Drosophila* and also in rodent models (Kim et al., 2012; Moroni et al., 2018; Zhang et al., 2019).

c) An interplay between Latrophilin and Teneurins was described recently in mammalians (Sando et al., 2019). In invertebrates, however, such interaction is not yet proven. Since Teneurins are highly conserved across phyla, published results – e.g. alternative spliced regions of *Ten2* may act as a switch to transcellular adhesion between Ten2 and Latrophilin (Li et al., 2018) and synaptogenesis is mediated by a an interplay of Latrophilin with FLRTs and Teneurins – are the base for future analysis. As FLRTs don't exist in *Drosophila*, Teneurins are a potential interaction partner of CIRL and should therefore be investigated in the future also in the context of mechanosensation.

d) Two-pore-domain potassium channels (K_2P) might also be potential candidates. In D*rosophila* two members of the TWIK-related acid-sensitive K_+ (TASK) family are expressed (dTASK6 & dTASK7) and where shown to sense mechanical force (Döring et al., 2006; Brohawn, 2015).

e) Moreover, transient receptor potential (TRP) channels are involved in recognizing a broad range of mechanical and chemical stimuli (Julius et al., 2001; Padinjat, 2004; Montell, 2005; Neely et al., 2011; Ferrandiz-Huertas et al., 2014). Scholz and coworkers have already hypothesized a model, in which CIRL inversely modulates inotropic gating characteristics of the mechanotransduction cascade involving NompC (TRPN channel) and Nanchung (TRPV channel) (Scholz et al., 2015). This was tested by combining *dCirl_{KO}* with hypomorphic mutants *nompc_{f00642}* and *nan_{36a}*, resulting in decreased (*nompc + dCirl* double mutant) and increased (*nanchung + dCirl* double mutant) larval crawling distance (Scholz et al., 2015). Furthermore, investigations on TRP/aGPCR interplay are

part of current work. Here, detailed analysis will show if TRP channels are directly modulated through the aGPCR CIRL or if they act in a signal cascade with different signaling steps in between. This is feasible by combing behavioral paradigms, immunohistochemistry and electrophysiology. Mutants or pharmacological assays to generate malfunctioning post translational modifications, like disrupted phosphorylation sites, of TRP channels can be employed in this context (Voolstra et al., 2014).

f) Potential GPCR–TRP channel interactions can be mediated by PKA (protein kinase A) and PKC (protein kinase C) depended TRP phosphorylation and thereby regulate channel open probabilities (Yekkirala, 2013; Veldhuis et al., 2014). Also coupling to $G\alpha$ proteins is a possible interaction mechanisms of aGPCRs (Inanobe et al., 2014; Langenhan, 2019; Röthe et al., 2019). Recently it was shown that in mammalian pancreatic β cells insulin segregation is regulated by Latrophilins. Thereby LPHN1 couples to a $G\alpha s$ protein and induces cAMP production – enhancing insulin secretion – whereas LPHN3 is able to decrease intracellular cAMP levels via $G\alpha i$ interaction – reducing insulin release (Röthe et al., 2019). By doing so, Latrophilins (LPHN1 & 3) tune the regulation of insulin release in mammals in an contrary way.

5.2 CIRL in a Taxol-induced peripheral neuropathy model

Over the last years, and for sure for the next time, neuropathy and cancer are huge research topics (Bray et al., 2012; Malvezzi et al., 2019). Beside work in rodent models also in *Drosophila,* new goals concerning a better understanding of ongoing physiological processes have been achieved.

In the second part of the thesis, CIRL function should be studied in a pathological context by employing a drug induced peripheral neuropathy model. At this juncture, we are going to give our results clinical relevance and they can be used as a base for rodent models and later be transferred to humans as well.

Some chemotherapeutic drugs, such as Taxol, cause IPN in a dose-depended manner thus limiting its applicability. In humans, hyperalgesia, hypoalgesia or allodynia are common side effects (Stillman et al., 2008; Sommer, 2016; Bussmann et al., 2017; Fukuda et al., 2017; Miaskowski et al., 2017). To resolve a better understanding of these mechanism, and to combine our previous findings with this new approach, we investigated the influence of CIRL on Taxol-induced phenotypes.

After *Drosophila* larvae were treated with the microtubule-stabilizing agent Taxol, we observed swelling, fragmentation, and loss of peripheral sensory fibers, without inducing apoptosis which is similar to previous work (Bhattacharya et al., 2012). Quantitative morphological analysis of C4da sensory neurons demonstrated a significant decrease in whole dendritic length and the number of terminals respectively. Some reports claim reduced larval area and dendritic size as well, but no altered or even increased number of branches and terminals (Brazill et al., 2018; Hamoudi et al., 2018). Notably hereby is, that the timepoint and duration of drug application, as well as the used solvent (vehicle) is crucial. Work from the DiAntonio lab demonstrated that injuries were apparent as early as 72 h with a maximum neuronal damage after 96 h upon Taxol application (Bhattacharya et al., 2012). Furthermore DMSO is more efficient in delivering drugs through membranes compared to EtOH (Davies et al., 2015). In studies examined no or minor changes of C4da morphology after Taxol treatment, timing or vehicle conditions were different (EtOH was used as vehicle and drug application was carried out for 48 h or less) compared to our results. This parameters would cause the differences between

the results from Hamoudi and Brazill compared to the results from us and the DiAntonio lab.

The influence of Taxol on nocifensive behavior was severe compared to control conditions. Different concentration of Taxol (10 – 40 µM) caused hyperalgesia-like responses of larvae upon mechanical stimulation. Interestingly, investigations on *dCirl* OE animals revealed a reduced response behavior despite Taxol application. On one hand this goes along with previous findings of *dCirl* OE resulting in hypoalgesia-like behavior, on the other hand it is astonishing how efficient the behavioral responses were rescued.

While behavior can be rescued by OE of CIRL, morphology analysis reveals no rescue of dendritic fibers. Strahler analysis showed a decrease in total branch numbers upon drug treatment, but a shift towards higher ordered branches. This suggests that remaining dendrites branch more, which might demonstrate a compensatory effect due to loss of field coverage.

Interestingly, our findings fit perfectly in data from rodent models. Heike Rittner (University Clinic Würzburg) and coworkers found a significant reduction of the aGPCR Cirl-1, the mammalian homolog of dCIRL, in rats' dorsal root ganglia one week after chronic constriction injury (CCI) (unpublished data). Rats suffer from neuropathic pain after CCI (Bennett et al., 2003), which results in hyperalgesia. This supports the notion that also in rodents, CIRL might be a key player in mechanosensation and a loss of CIRL results in a stronger nocifensive behavior.

6 Conclusion and outlook

Taken together, in this thesis a novel functional role of the aGPCR Latrophilin/dCirl in *Drosophila* was shown. Employing behavioral paradigms, immunohistochemistry, optogenetics and calcium imaging, it could be demonstrated that dCirl is expressed in peripheral larval nociceptors (Type II Class IV multidendritic sensory neurons), where it functions as a down-regulator of nocifensive behavior by modulating nocifensive neurons via second messenger pathways involving cAMP.

Thus, a loss of CIRL and elevated cAMP levels give rise to hyperalgesia in null mutations (*dCirlKO*) as well as cell specific knockdowns (*dCirlRNAi*). Investigations on cleavage deficient mutants uncovered that a punctmutation within the tethered agonist *Stachel* is negligible but a punctual mutation at the beginning of the NTF lead to hyperalgesia. In contrast, cell specific OE of *dCirl* in nociceptors (C4da neurons), rescued exuberant nocifensive behavior in the knockout background and reduced behavioral response even further in the wildtype background.

Together with previous result from lch5 chordotonal organs (Scholz et al., 2015, 2017), we found that CIRL exerts opposing modulatory effects in low-threshold mechanosensory neurons (lch5) and high-threshold nociceptors (C4da). This bipolar action likely facilitates the differentiation of noxious and innoxious mechanosensory signals carrying different physiological information in a cell specific manner (Figure 22).
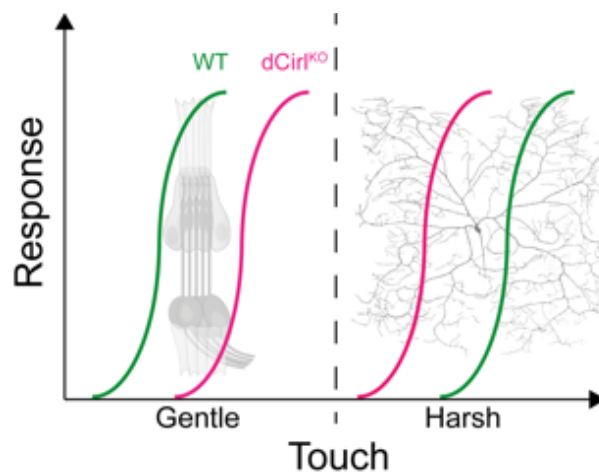

Figure 22. CIRL shapes mechanosensation in a highly cell specific manner. Our results from noxious mechanosensors together with the results obtained from ChO (Scholz et al., 2017), we suppose cell specific function of CIRL in mechanosensation. While in low threshold mechanoreceptors (chordotonal organs), a loss of CIRL results in a loss of mechanosensation, in high-threshold nociceptors (C4da) loss of CIRL implicates hyper sensation to mechanical stimuli. This gives evidence for CIRL acting as a signal discriminator.

Moreover, given the clinical relevance of this results, we made use of a drug induced toxic neuropathy model in order to test for CIRL function in this context. Taxol treatment induces morphological neuropathy and hyperalgesia in *Drosophila* larvae. Analysis revealed, that cell specific OE of *dCirl* counteracts the hyperalgesia in an analgesic like manner, however, does not rescue the morphological defects of nociceptive neurons.

Subsequent experiments could include pharmacological inhibitors of adenylyl cyclase activity to test for an potential rescue of neuronal function in *dCirl* knockout animals and in the IPN model. Moreover, a genetical screen could be applied with ease to identify potential interaction partners of *dCirl,* but also to reveal key players in mechanosensation. Furthermore, a synthesized *Stachel* peptide or different types of mutations concerning CTF and NTF function can be used to test for an involvement in mechanosensation as well as in the IPN model.

By doing so, it can be clarified if an intact NTF exclusively is necessary for proper CIRL function in nociceptors and if a synthetic peptide is able to provoke a reduction in nocifensive response upon noxious touch and Taxol application. Potential outcomes can then be transferred back to pain resolution models in rodents and patients. Thereby a base for potent analgesic drugs can be created.

Nociceptive perception is a hallmark of mechanosensory system and should therefore a major interest in prospective work. This becomes obvious since many diseases in humans involve neuronal disorders connected to mechanosensation. Given this importance it seems surprising, that investigations concerning the processes and pathways involved in sensing and integrating mechanical stimuli are still not understood in detail. Therefore, further research regarding this topic, will generate a better understanding of aGPCR function and pharmacological drugs based on future discoveries.

7 Supplementary data

Colors mark experimental data set. Each top line is used as control respectively. Values represent mean ± SEM. N indicates the total number of tested larvae represented by n.

Suppl. Table 1. Quantification of different von-Frey-filaments with forces between 20 mN - 50 mN.

Genotype	Force	Nocifensive response (%) ± SEM	n	N
w_{1118}	20 mN	13.33 ± 2.36	5	150
	30 mN	36.67 ± 2.36	5	150
	40 mN	53.22 ± 1.13	5	166
	50 mN	78.67 ± 3.09	5	150

Suppl. Table 2. Statistics of behavior nociception assay. Related to Figure 15. *P* values shown were generated using unpaired, parametric t-test.

Genotype	Nocifensive response (%) ± SEM	n	N	*P*
$dCirl_{Rescue}$	53.34 ± 1.46	7	218	-
$dCirl_{KO}$	75.37 ± 2.68	10	290	< 0.0001
ppk_{GAL4} / +	50.14 ± 3.97	10	268	-
$dCirl_{RNAi}$/+	54.23 ± 3.28	8	249	0.4541
ppk_{GAL4} / $dCirl_{RNAi}$	68.08 ± 2.05	10	252	0.0008
$dCirl_{Rescue}$	54.28 ± 1.96	10	203	-
$dCirl_{T>A}$	55.00 ± 2.27	10	208	0.8130
$dCirl_{H>A}$	73.78 ± 1.85	10	475	< 0.0001
$dCirl_{Rescue}$ /+ , ppk_{GAL4} /+	53.70 ± 3.20	14	365	-
$dCirl_{KO}$, ppk_{GAL4} / +	75.30 ± 2.20	12	318	< 0.0001
$dCirl_{KO}$, ppk_{GAL4} / UAS-dCirl	45.70 ± 3.60	10	230	0.1169
ppk_{GAL4} / UAS-dCirl	37.01 ± 2.80	10	307	0.0013
ppk_{GAL4} / UAS-dCirl @29 °C	28.70 ± 3.10	10	209	< 0.0001

Suppl. Table 3. Quantification of dendritic length (mm). Related to Figure 16. *P* values shown were generated using unpaired, parametric t-test.

Genotype	Dendritic length (mm)	n	*P*
dCirl_{Rescue}	18.11 ± 0.50	8	-
dCirl_{KO}	17.37 ± 0.44	10	0.2829

Suppl. Table 4. Quantification of C4da terminals. Related to Figure 16. *P* values shown were generated using unpaired, parametric t-test.

Genotype	# of terminals (x100)	n	*P*
dCirl_{Rescue}	4.971 ± 0.1747	8	-
dCirl_{KO}	4.219 ± 0.1255	10	0.0025

Suppl. Table 5. Statistics of behavior nociception of PDE mutants. Related to Figure 17. *P* values shown were generated using unpaired, nonparametric Mann-Whitney U test.

Genotype	Nocifensive response (%) $\pm$ SEM	n	N	*P*
canton S	44.00 ± 3.71	10	200	-
dunce₁	72.00 ± 1.11	10	200	< 0.0001
w,y, f_{36a}	50.50 ± 1.17	10	200	-
dunce_{ML}	79.60 ± 0.97	12	240	< 0.0001

Suppl. Table 6. Statistics of behavior optogenetic nociception assay. Related to Figure 17.

Genotype	Condition	Score distribution 0 (n / %)	1 (n / %)	2 (n / %)	3 (n / %)	Σ n
w₁₁₁₈	dark	96 / 47.29	107 / 52.71	0 / 0	0 / 0	203
	light	96 / 48.00	104 / 52.00	0 / 0	0 / 0	200
UAS-bPAC / +	dark	40 / 40.00	54 / 54.00	6 / 6.00	0 / 0	100
	light	36 / 36.00	56 / 56.00	8 / 8.00	0 / 0	100
ppk_{GAL4} / UAS-bPAC	dark	30 / 31.25	51 / 53.13	15 / 15.63	0 / 0	96
	light	2 / 5.13	22 / 56.41	11 / 28.21	4 / 10.26	39

dCirl_{KO}; ppk_{GAL4} / UAS-bPAC	dark	0 / 0	21 / 70.00	8 / 26.67	1 / 3.33	30
	light	0 / 0	18 / 58.06	4 / 12.90	9 / 29.03	31

Suppl. Table 7. Quantification of peak ΔF/F. Related to Figure 19. *P* values shown were generated using unpaired, parametric t-test.

Genotype	Peak ΔF/F	n	*P*
ppkGAL4; UAS-GCaMP6	0.006962 ± 0.001546	11	-
dCirl_{KO}, ppkGAL4; UAS-GCaMP6	0.0229 ± 0.003518	10	0.0004

Suppl. Table 8. Quantification of quotient from peak ΔF/F in relation to baseline $(\Delta F/F)_0$. Related to Figure 19. *P* values shown were generated using unpaired, parametric t-test.

Genotype	(Peak ΔF/F)/$(\Delta F/F)_0$	n	*P*
ppkGAL4; UAS-GCaMP6	42.20 ± 22.71	11	-
dCirl_{KO}, ppkGAL4; UAS-GCaMP6	115.50 ± 51.88	10	0.0231

Suppl. Table 9. Statistics of behavior nociception assay from the Taxol IPN model. Influence of different Taxol and DMSO (vehicle) concentrations on nocifensive behavior. Related to Figure 20. *P* values shown were generated using unpaired, nonparametric Mann-Whitney U test.

Condition	Nocifensive response (%) ± SEM	n	N	*P*
DMSO (10 µl)	53.96 ± 3.831	19	398	-
Taxol (10 µM)	95.50 ± 1.740	10	170	< 0.0001
DMSO (20 µl)	54.77 ± 3.867	10	200	-
Taxol (20 µM)	99.17 ± 0.833	6	143	< 0.0001
DMSO (40 µl)	52.28 ± 3.442	8	122	-
Taxol (40 µM)	99.05 ± 0.614	7	110	< 0.0001

Suppl. Table 10. Statistics of behavior nociception assay from the Taxol IPN model and the influence of dCirl OE. Related to Figure 21. *P* values shown were generated using unpaired, nonparametric Mann-Whitney U test.

Genotype	Condition	Nocifensive response (%) ± SEM	n	N	*P*
*ppk*GAL4 / +	DMSO	53.96 ± 3.83	19	398	-
*ppk*GAL4 / +	Taxol	95.50 ± 1.74	10	170	< 0.0001
*dCirl*KO	DMSO	69.68 ± 3.54	20	425	-
*dCirl*KO	Taxol	97.05 ± 1.10	10	188	< 0.0001
*ppk*GAL4 / UAS-dCirl	DMSO	37.12 ± 2.78	10	307	-
*ppk*GAL4 / UAS-dCirl	Taxol	46.34 ± 2.37	10	205	0.021

Suppl. Table 11. Quantification of dendritic length (mm) under Taxol treatment. Related to Figure 21., *P* values shown were generated using unpaired, parametric t-test.

Genotype	Condition	Dendritic length (mm)	n	*P*
*ppk*GAL4 / +	DMSO	22.17 ± 0.7015	10	-
*ppk*GAL4 / +	Taxol	15.42 ± 1.174	10	< 0.0001
*ppk*GAL4 / UAS-dCirl	DMSO	17.26 ± 0.6091	10	-
*ppk*GAL4 / UAS-dCirl	Taxol	11.22 ± 1.716	10	0.0147

Suppl. Table 12. Quantification of dendritic length (mm) under Taxol treatment. Related to Figure 21. *P* values shown were generated using unpaired, nonparametric Mann-Whitney U test.

Genotype	Condition	# of terminals (x100)	n	*P*
*ppk*GAL4 / +	DMSO	8.26 ± 0.198	10	-
*ppk*GAL4 / +	Taxol	6.27 ± 0.557	10	0.0035
*ppk*GAL4 / UAS-dCirl	DMSO	5.11 ± 0.160	10	-
*ppk*GAL4 / UAS-dCirl	Taxol	3.86 ± 0.596	10	0.0585

8 References

Adams CM, Anderson MG, Motto DG, Price MP, Johnson WA, Welsh MJ (1998) Ripped pocket and pickpocket, novel *Drosophila* DEG/ENaC subunits expressed in early development and in mechanosensory neurons. J Cell Biol 140:143–152.

Adams J (2004) The proteasome: a suitable antineoplastic target. Nat Rev Cancer 4:349–360.

Araç D, Sträter N, Seiradake E (2016) Understanding the Structural Basis of Adhesion GPCR Functions. In: Encyclopedia of Signaling Molecules, pp 67–82.

Arcos-Burgos M et al. (2010) A common variant of the latrophilin 3 gene, LPHN3, confers susceptibility to ADHD and predicts effectiveness of stimulant medication. Mol Psychiatry 15:1053–1066.

Argyriou AA, Kyritsis AP, Makatsoris T, Kalofonos HP (2014) Chemotherapy-induced peripheral neuropathy in adults: a comprehensive update of the literature. Cancer Manag Res 6:135–147.

Ashburner M, Roote J (2007) Culture of *Drosophila*: The Laboratory Setup. Cold Spring Harb Protoc 2007.

Aust G, Zhu D, Van Meir EG, Xu L (2016) Adhesion GPCRs in Tumorigenesis. Handb Exp Pharmacol 234:369–396.

Basith S, Cui M, Macalino SJY, Park J, Clavio NAB, Kang S, Choi S (2018) Exploring G protein-coupled receptors (GPCRs) ligand space via cheminformatics approaches: Impact on rational drug design. Front Pharmacol 9:1–26.

Bazopoulou D, Voglis G, Tavernarakis N (2007) The role of DEG/ENaC ion channels in sensory mechanotransduction. Mol Sensors Cardiovasc Homeost:3–31.

Beliu G, Kurz A, Kuhlemann A, Behringer-Pliess L, Wolf N, Seibel J, Shi Z-D, Schnermann M, Grimm JB, Lavis LD, Doose S, Sauer M (2018) Bioorthogonal labeling with tetrazine-dyes for super-resolution microscopy. bioRxiv:503821.

Bennett GJ, Chung JM, Honore M, Seltzer Z (2003) Models of Neuropathic Pain in the Rat. Curr Protoc Neurosci 22:9.14.1-9.14.16.

Bhattacharya MRC, Gerdts J, Naylor SA, Royse EX, Ebstein SY, Sasaki Y, Milbrandt J, DiAntonio A (2012) A Model of Toxic Neuropathy in *Drosophila* Reveals a Role for MORN4 in Promoting Axonal Degeneration. J Neurosci 32:5054–5061.

Bockaert J (1999) Molecular tinkering of G protein-coupled receptors: an evolutionary success. EMBO J 18:1723–1729.

Bodmer R, Carretto R, Jan YN (1989) Neurogenesis of the peripheral nervous system in *Drosophila* embryos: DNA replication patterns and cell lineages. Neuron 3:21–32.

Boyden SE et al. (2016) Vibratory Urticaria Associated with a Missense Variant in ADGRE2. N Engl J Med 374:656–663.

Brace EJ, DiAntonio A (2017) Models of axon regeneration in *Drosophila*. Exp Neurol 287:310–317.

Brand AH, Perrimon N (1993) Targeted gene expression as a means of altering cell fates and generating dominant phenotypes. Development 118:401–415.

Bray F, Jemal A, Grey N, Ferlay J, Forman D (2012) Global cancer transitions according to the Human Development Index (2008-2030): A population-based study. Lancet Oncol 13:790–801.

Brazill JM, Cruz B, Zhu Y, Zhai RG (2018) Nmnat mitigates sensory dysfunction in a *Drosophila* model of paclitaxel-induced peripheral neuropathy. Dis Model Mech 11:dmm032938.

Brohawn SG (2015) How ion channels sense mechanical force: Insights from mechanosensitive K2P channels TRAAK, TREK1, and TREK2. Ann N Y Acad Sci 1352:20–32.

Broussard GJ, Liang R, Tian L (2014) Monitoring activity in neural circuits with genetically encoded indicators. Front Mol Neurosci 7.

Bussmann J, Storkebaum E (2017) Molecular pathogenesis of peripheral neuropathies: insights from *Drosophila* models. Curr Opin Genet Dev 44:61–73.

Carton Y, Boulétreau M, van Alphen JJM, van Lenteren JC (1986) The *Drosophila* Parasitic Wasps. Genet Biol *Drosophila*:347–394.

Cashman CR, Höke A (2015) Mechanisms of distal axonal degeneration in peripheral neuropathies. Neurosci Lett 596:33–50.

Cheng LE, Song W, Looger LL, Jan LY, Jan YN (2010) The Role of the TRP Channel NompC in *Drosophila* Larval and Adult Locomotion. Neuron 67:373–380.

Chin MR, Tracey WD (2017) Nociceptive Circuits: Can't Escape Detection. Curr Biol 27:R796–R798.

Coleman M (2005) Axon degeneration mechanisms: Commonality amid diversity. Nat Rev Neurosci 6:889–898.

Coste B, Mathur J, Schmidt M, Earley TJ, Ranade S, Petrus MJ, Dubin AE, Patapoutian A (2010) Piezo1 and Piezo2 Are Essential Components of Distinct Mechanically Activated Cation Channels. Science (80-) 330:55 LP – 60.

Coste B, Xiao B, Santos JS, Syeda R, Grandl J, Spencer KS, Kim SE, Schmidt M, Mathur J, Dubin AE, Montal M, Patapoutian A (2012) Piezo proteins are pore-forming subunits of mechanically activated channels. Nature 483:176.

Dahmann C (2008) *Drosophila* (Dahmann C, ed). Totowa, NJ: Humana Press.

Davies J, Ingham A (2015) An in-vitro-in-vivo model for the transdermal delivery of cholecalciferol for the purposes of rodent management. Int J Pharm 487:101–109.

Davis RL, Kiger JA (1981) Dunce Mutants of *Drosophila melanogaster*: mutants defective in the cyclic AMP phosphodiesterase enzyme system. J Cell Biol 90:101–107.

Davletov BA, Shamotienko OG, Lelianova VG, Grishin E V., Ushkaryov YA (1996) Isolation and biochemical characterization of a Ca_{2+}-independent α-latrotoxin-binding protein. J Biol Chem 271:23239–23245.

Dietzl G, Chen D, Schnorrer F, Su KC, Barinova Y, Fellner M, Gasser B, Kinsey K, Oppel S, Scheiblauer S, Couto A, Marra V, Keleman K, Dickson BJ (2007) A genome-wide transgenic RNAi library for conditional gene inactivation in *Drosophila*. Nature 448:151–156.

Domené S, Stanescu H, Wallis D, Tinloy B, Pineda DE, Kleta R, Arcos-Burgos M, Roessler E, Muenke M (2011) Screening of human LPHN3 for variants with a potential impact on ADHD susceptibility. Am J Med Genet Part B Neuropsychiatr Genet 156:11–18.

Döring F, Scholz H, Kühnlein RP, Karschin A, Wischmeyer E (2006) Novel *Drosophila* two-pore domain K_+ channels: Rescue of channel function by heteromeric assembly. Eur J Neurosci 24:2264–2274.

Duffy JB (2002) GAL4 system in *Drosophila*: a fly geneticist's Swiss army knife. Genesis 34:1–15.

Ehmann N, van de Linde S, Alon A, Ljaschenko D, Keung XZ, Holm T, Rings A, DiAntonio A, Hallermann S, Ashery U, Heckmann M, Sauer M, Kittel RJ (2014) Quantitative super-resolution imaging of Bruchpilot distinguishes active zone states. Nat Commun 5:4650.

Ferrandiz-Huertas C, Mathivanan S, Wolf CJ, Devesa I, Ferrer-Montiel A (2014) Trafficking of Thermo TRP channels. Membranes (Basel) 4:525–564.

Flower DR (1999) Modelling G-protein-coupled receptors for drug design. Biochim Biophys Acta - Rev Biomembr 1422:207–234.

Fredriksson R (2005) The Repertoire of G-Protein-Coupled Receptors in Fully Sequenced Genomes. Mol Pharmacol 67:1414–1425.

Fukuda Y, Li Y, Segal RA (2017) A mechanistic understanding of axon degeneration in chemotherapy-induced peripheral neuropathy. Front Neurosci 11:1–12.

Gorczyca DA, Younger S, Meltzer S, Kim SE, Cheng L, Song W, Lee HY, Jan LY, Jan YN (2014) Identification of Ppk26, a DEG/ENaC Channel Functioning with Ppk1 in a Mutually Dependent Manner to Guide Locomotion Behavior in *Drosophila*. Cell Rep 9:1446–1458.

Grueber WB, Ye B, Moore AW, Jan LY, Jan YN (2003) Dendrites of Distinct Classes of *Drosophila* Sensory Neurons Show Different Capacities for Homotypic Repulsion. Curr Biol 13:618–626.

Grueber WB, Ye B, Yang C-H, Younger S, Borden K, Jan LY, Jan Y-N (2006) Projections of *Drosophila* multidendritic neurons in the central nervous system: links with peripheral dendrite morphology. Development 134:55–64.

Guo Y, Wang Y, Wang Q, Wang Z (2014) The Role of PPK26 in *Drosophila* Larval Mechanical Nociception. Cell Rep 9:1183–1190.

Hales KG, Korey CA, Larracuente AM, Roberts DM (2015) Genetics on the fly: A primer on the *Drosophila* model system. Genetics 201:815–842.

Hamoudi Z, Khuong TM, Cole T, Neely GG (2018) A fruit fly model for studying paclitaxel-induced peripheral neuropathy and hyperalgesia. F1000Research 7:99.

Han C, Jan LY, Jan Y-N (2011) Enhancer-driven membrane markers for analysis of nonautonomous mechanisms reveal neuron-glia interactions in *Drosophila*. Proc Natl Acad Sci 108:9673–9678.

Herr K, Gibson S, Hadjistavropoulos T (2017) Pain. In: The Wiley Handbook on the Aging Mind and Brain (Abd-Elsayed A, ed), pp 628–647. Cham: Springer International Publishing.

Honjo K, Mauthner SE, Wang Y, Skene JHHP, Tracey WD (2016) Nociceptor-Enriched Genes Required for Normal Thermal Nociception. Cell Rep 16:295–303.

Hoyer N, Petersen M, Tenedini F, Soba P (2018) Assaying Mechanonociceptive Behavior in *Drosophila* Larvae. Bio-Protocol 8:1–13.

Hu C, Petersen M, Hoyer N, Spitzweck B, Tenedini F, Wang D, Gruschka A, Burchardt LS, Szpotowicz E, Schweizer M, Guntur AR, Yang C-H, Soba P (2018) Modality-specific sensory integration and neuropeptide- mediated feedback facilitate mechano-nociceptive behavior in *Drosophila*. 20:1085–1095.

Hughes CL, Thomas JB (2007) A sensory feedback circuit coordinates muscle activity in *Drosophila*. Mol Cell Neurosci 35:383–396.

Hwang RY, Zhong L, Xu Y, Johnson T, Zhang F, Deisseroth K, Tracey WD (2007) Nociceptive Neurons Protect *Drosophila* Larvae from Parasitoid Wasps. Curr Biol 17:2105–2116.

Ichtchenko K, Bittner MA, Krasnoperov V, Little AR, Chepurny O, Holz RW, Petrenko AG (1999) A novel ubiquitously expressed α-latrotoxin receptor is a member of the CIRL family of G-protein-coupled receptors. J Biol Chem 274:5491–5498.

Im SH, Galko MJ (2012) Pokes, sunburn, and hot sauce: *Drosophila* as an emerging model for the biology of nociception. Dev Dyn 241:16–26.

Inanobe A, Kurachi Y (2014) Membrane channels as integrators of G-protein-mediated signaling. Biochim Biophys Acta - Biomembr 1838:521–531.

Islam S (2011) Transient Receptor Potential Channels, Shahidul I. Dordrecht: Springer Netherlands.

Jarosch B, Jarosch B (2018) Neuro- und Sinnesphysiologie.

Johnston DS (2002) the Art and Design of Genetic Screens : *Drosophila melanogaster*. 3:176–188.

Johnstone TC, Park GY, Lippard SJ (2014) Understanding and improving platinum anticancer drugs--phenanthriplatin. Anticancer Res 34:471–476.

Jordan MA, Wilson L (2004) Microtubules as a target for anticancer drugs. Nat Rev Cancer 4:253–265.

Julius D, Basbaum AI (2001) Molecular mechanisms of nociception. Nature 413:203–210.

Khuong TM, Wang Q, Manion J, Oyston LJ, Lau M, Towler H, Lin YQ, Neely GG (2019) Nerve injury drives a heightened state of vigilance and neuropathic sensitization in *Drosophila*. Sci Adv 5:eaaw4099.

Kim M-J, Johnson WA (2014) ROS-mediated activation of *Drosophila* larval nociceptor neurons by UVC irradiation. BMC Neurosci 15:14.

Kim SE, Coste B, Chadha A, Cook B, Patapoutian A (2012) The role of *Drosophila* Piezo in mechanical nociception. Nature 483:209–212.

Kim SH, Lee Y, Akitake B, Woodward OM, Guggino WB, Montell C (2010) *Drosophila* TRPA1 channel mediates chemical avoidance in gustatory receptor neurons. Proc Natl Acad Sci 107:8440–8445.

Kishore A, Hall RA (2016) Versatile Signaling Activity of Adhesion GPCRs. In: Encyclopedia of Signaling Molecules, pp 127–146.

Kobilka BK, Deupi X (2007) Conformational complexity of G-protein-coupled receptors. Trends Pharmacol Sci 28:397–406.

Kovacs P, Schöneberg T (2016) The Relevance of Genomic Signatures at Adhesion GPCR Loci in Humans. In: Encyclopedia of Signaling Molecules, pp 179–217.

Krasnoperov VG, Bittner MA, Beavis R, Kuang Y, Salnikow K V., Chepurny OG, Little AR, Plotnikov AN, Wu D, Holz RW, Petrenko AG (1997) α-Latrotoxin stimulates exocytosis by the interaction with a neuronal G-protein-coupled receptor. Neuron 18:925–937.

Krishnan A, Nijmeijer S, de Graaf C, Schiöth HB (2016) Classification, Nomenclature, and Structural Aspects of Adhesion GPCRs. In: Encyclopedia of Signaling Molecules, pp 15–41.

Kwan KY, Corey DP (2009) Burning Cold: Involvement of TRPA1 in Noxious Cold Sensation. J Gen Physiol 133:251–256.

Lai S-L, Lee T (2006) Genetic mosaic with dual binary transcriptional systems in *Drosophila*. Nat Neurosci 9:703–709.

Langenhan T (2019) Adhesion G protein–coupled receptors—Candidate metabotropic mechanosensors and novel drug targets. Basic Clin Pharmacol Toxicol 1:1–12.

Langenhan T, Aust G, Hamann J (2013) Sticky signaling - Adhesion class g protein-coupled receptors take the stage. Sci Signal 6:1–22.

Langenhan T, Piao X, Monk KR (2016) Adhesion G protein-coupled receptors in nervous system development and disease. Nat Rev Neurosci 17:550–561.

Langenhan T, Prömel S, Mestek L, Esmaeili B, Waller-Evans H, Hennig C, Kohara Y, Avery L, Vakonakis I, Schnabel R, Russ AP (2009) Latrophilin Signaling Links Anterior-Posterior Tissue Polarity and Oriented Cell Divisions in the C. elegans Embryo. Dev Cell 17:494–504.

Ledderose J, Sención L, Salgado H, Arias-Carrión O, Treviño M (2014) A software tool for the analysis of neuronal morphology data. Int Arch Med 7:1–9.

Li J, Shalev-Benami M, Sando R, Jiang X, Kibrom A, Wang J, Leon K, Katanski C, Nazarko O, Lu YC, Südhof TC, Skiniotis G, Araç D (2018) Structural Basis for Teneurin Function in Circuit-Wiring: A Toxin Motif at the Synapse. Cell 173:735-748.e15.

Liebscher I et al. (2014a) New functions and signaling mechanisms for the class of adhesion G protein-coupled receptors. Ann N Y Acad Sci 1333:43–64.

Liebscher I, Schön J, Petersen SC, Fischer L, Auerbach N, Demberg LM, Mogha A, Cöster M, Simon KU, Rothemund S, Monk KR, Schöneberg T (2014b) A Tethered Agonist within the Ectodomain Activates the Adhesion G Protein-Coupled Receptors GPR126 and GPR133. Cell Rep 9:2018–2026.

Liebscher I, Schöneberg T (2016) Tethered Agonism: A Common Activation Mechanism of Adhesion GPCRs. In: Encyclopedia of Signaling Molecules, pp 111–125.

Liebscher I, Schöneberg T, Prömel S (2013) Progress in demystification of adhesion G protein-coupled receptors. Biol Chem 394:937–950.

Lin HH, Hsiao CC, Pabst C, Hébert J, Schöneberg T, Hamann J (2017) Adhesion GPCRs in Regulating Immune Responses and Inflammation. Adv Immunol 136:163–201.

Lindsley DL, Grell EH (1968) Genetic Variations of *Drosophila melanogaster*.

Ljaschenko D, Ehmann N, Kittel RJ (2013) Hebbian Plasticity Guides Maturation of Glutamate Receptor Fields InVivo. Cell Rep 3:1407–1413.

Loeser JD, Treede R-D (2008) The Kyoto protocol of IASP Basic Pain Terminology☆. Pain 137:473–477.

Lumpkin EA, Marshall KL, Nelson AM (2010) The cell biology of touch. J Cell Biol 191:237–248.

Lundstrom K (2006) Latest Development in Drug Discovery on G Protein-coupled Receptors. Curr Protein Pept Sci 7:465–470.

Maiellaro I, Lohse MJ, Kittel RJ, Calebiro D (2016) cAMP Signals in *Drosophila* Motor Neurons Are Confined to Single Synaptic Boutons. Cell Rep 17:1238–1246.

Malvezzi M, Carioli G, Bertuccio P, Boffetta P, Levi F, La Vecchia C, Negri E (2019) European cancer mortality predictions for the year 2019 with focus on breast cancer. Ann Oncol Off J Eur Soc Med Oncol 30:781–787.

Marasco A, Limongiello A, Migliore M (2013) Using Strahler's analysis to reduce up to 200-fold the run time of realistic neuron models. Sci Rep 3:1–7.

Mauthner SE, Hwang RY, Lewis AH, Xiao Q, Tsubouchi A, Wang Y, Honjo K, Skene JHP, Grandl J, Tracey WD (2014) Balboa binds to pickpocket in vivo and is required for mechanical nociception in *Drosophila* larvae. Curr Biol 24:2920–2925.

Miaskowski C, Mastick J, Paul SM, Topp K, Smoot B, Abrams G, Chen L-M, Kober KM, Conley YP, Chesney M, Bolla K, Mausisa G, Mazor M, Wong M, Schumacher M, Levine JD (2017) Chemotherapy-Induced Neuropathy in Cancer Survivors. J Pain Symptom Manage 54:204-218.e2.

Milinkeviciute G, Gentile C, Neely GG (2012) *Drosophila* as a tool for studying the conserved genetics of pain. Clin Genet 82:359–366.

Montell C (2005) *Drosophila* TRP channels. Pflugers Arch Eur J Physiol 451:19–28.

Montgomery MK, Xu S, Fire a (1998) RNA as a target of double-stranded RNA-mediated genetic interference in Caenorhabditis elegans. Proc Natl Acad Sci U S A 95:15502–15507.

Moroni M, Servin-Vences MR, Fleischer R, Sánchez-Carranza O, Lewin GR (2018) Voltage gating of mechanosensitive PIEZO channels. Nat Commun 9:1–15.

Müller A, Winkler J, Fiedler F, Sastradihardja T, Binder C, Schnabel R, Kungel J, Rothemund S, Hennig C, Schöneberg T, Prömel S (2015) Oriented Cell Division in the C. elegans Embryo Is Coordinated by G-Protein Signaling Dependent on the Adhesion GPCR LAT-1. PLoS Genet 11:1–20.

National Research Council (2009) Recognition and Alleviation of Pain in Laboratory Animals.

Neely GG, Keene AC, Duchek P, Chang EC, Wang QP, Aksoy YA, Rosenzweig M, Costigan M, Woolf CJ, Garrity PA, Penninger JM (2011) TrpA1 regulates thermal nociception in *Drosophila*. PLoS One 6.

Ni JQ, Liu LP, Binari R, Hardy R, Shim HS, Cavallaro A, Booker M, Pfeiffer BD, Markstein M, Wang H, Villalta C, Laverty TR, Perkins LA, Perrimon N (2009) A *Drosophila* resource of transgenic RNAi lines for neurogenetics. Genetics 182:1089–1100.

Nieberler M, Kittel RJ, Petrenko AG, Lin H-H, Langenhan T (2016) Control of Adhesion GPCR Function Through Proteolytic Processing. In: Encyclopedia of Signaling Molecules, pp 83–109. Cham: Springer International Publishing.

Nijmeijer S, Wolf S, Ernst OP, de Graaf C (2016) 7TM Domain Structure of Adhesion GPCRs. In: Encyclopedia of Signaling Molecules, pp 43–66.

O'Hayre M, Vázquez-Prado J, Kufareva I, Stawiski EW, Handel TM, Seshagiri S, Gutkind JS (2013) The emerging mutational landscape of G proteins and G-protein-coupled receptors in cancer. Nat Rev Cancer 13:412–424.

Padinjat R (2004) TRP channels at a glance. J Cell Sci 117:5707–5709.

Parrish JZ (2016) Tiling and Mosaic Spacing of Dendrites. In: Dendrites (Emoto K, Wong R, Huang E, Hoogenraad C, eds), pp 181–211. Tokyo: Springer Japan.

Paul MM, Pauli M, Ehmann N, Hallermann S, Sauer M, Kittel RJ, Heckmann M (2015) Bruchpilot and Synaptotagmin collaborate to drive rapid glutamate release and active zone differentiation. Front Cell Neurosci 9:29.

Pfeiffer BD, Ngo T-TB, Hibbard KL, Murphy C, Jenett A, Truman JW, Rubin GM (2010) Refinement of Tools for Targeted Gene Expression in *Drosophila*. Genetics 186:735 LP – 755.

Pierce KL, Premont RT, Lefkowitz RJ (2002) Seven-transmembrane receptors. Nat Rev Mol Cell Biol 3:639–650.

Potter CJ, Tasic B, Russler E V, Liang L (2010) The Q system. 141:536–548.

Prokop A (1999) Integrating bits and pieces: Synapse structure and formation in *Drosophila* embryos. Cell Tissue Res 297:169–186.

Prömel S, Frickenhaus M, Hughes S, Mestek L, Staunton D, Woollard A, Vakonakis I, Schöneberg T, Schnabel R, Russ AP, Langenhan T (2012) The GPS motif is a molecular switch for bimodal activfileities of adhesion class G protein-coupled receptors. Cell Rep 2:321–331.

Purcell RH, Hall RA (2018) Adhesion G Protein–Coupled Receptors as Drug Targets. Annu Rev Pharmacol Toxicol 58:429–449.

Reinhold AK, Batti L, Bilbao D, Buness A, Rittner HL, Heppenstall PA (2015) Differential transcriptional profiling of damaged and intact adjacent dorsal root ganglia neurons in neuropathic pain. PLoS One 10:e0123342–e0123342.

Röthe J, Thor D, Winkler J, Knierim AB, Binder C, Huth S, Kraft R, Rothemund S, Schöneberg T, Prömel S (2019) Involvement of the Adhesion GPCRs Latrophilins in the Regulation of Insulin Release. Cell Rep 26:1573-1584.e5.

Salz HK, Kiger JA (1984) Genetic analysis of chromomere 3D4 in *Drosophila melanogaster*. II. Regulatory sites for the dunce gene. Genetics 108:377–392.

Sando R, Jiang X, Südhof TC (2019) Latrophilin GPCRs direct synapse specificity by coincident binding of FLRTs and teneurins. Science (80-) 363:eaav7969.

Sapar ML, Han C (2019) Die in pieces: How *Drosophila* sheds light on neurite degeneration and clearance. J Genet Genomics.

Schmid A, Sigrist SJ (2008) Analysis of neuromuscular junctions: histology and in vivo imaging. Methods Mol Biol 420:239–251.

Schmidt R (2011) Physiologie des Menschen.

Scholz N (2018) Cancer Cell Mechanics: Adhesion G Protein-coupled Receptors in Action? Front Oncol 8.

Scholz N, Gehring J, Guan C, Ljaschenko D, Fischer R, Lakshmanan V, Kittel RJ, Langenhan T (2015) The Adhesion GPCR Latrophilin/CIRL Shapes Mechanosensation. Cell Rep 11:866–874.

Scholz N, Guan C, Nieberler M, Grotemeyer A, Maiellaro I, Gao S, Beck S, Pawlak M, Sauer M, Asan E, Rothemund S, Winkler J, Prömel S, Nagel G, Langenhan T, Kittel RJ (2017) Mechano-dependent signaling by latrophilin/CIRL quenches cAMP in proprioceptive neurons. Elife 6:1–21.

Scholz N, Monk KR, Kittel RJ, Langenhan T (2016) Adhesion GPCRs as a Putative Class of Metabotropic Mechanosensors. In: Encyclopedia of Signaling Molecules, pp 221–247. Cham: Springer International Publishing.

Schöneberg T, Prömel S (2019) Latrophilins and Teneurins in Invertebrates: No Love for Each Other? Front Neurosci 13:1–11.

Sherrington CS (1906) The integrative action of the nervous system. New York, C Scribner's sons.

Sholl DA (1953) Dendritic organization in the neurons of the visual and motor cortices of the cat. J Anat 87:387–406.

Sillar KT, Picton LD, Heitler WJ (2016) The Neuroethology of Predation and Escape.

Singhania A, Grueber WB (2014) Development of the embryonic and larval peripheral nervous system of *Drosophila*. Wiley Interdiscip Rev Dev Biol 3:193–210.

Sneddon LU (2004) Evolution of nociception in vertebrates: Comparative analysis of lower vertebrates. Brain Res Rev 46:123–130.

Sommer C (2016) Exploring pain pathophysiology in patients. Science (80-) 354:588–592.

Stahl SMCN-R. S 2013 (2013) Stahl's essential psychopharmacology: neuroscientific basis and practical application, 4th ed. Cambridge ; New York: Cambridge University Press.

Stierl M, Stumpf P, Udwari D, Gueta R, Hagedorn R, Losi A, G??rtner W, Petereit L, Efetova M, Schwarzel M, Oertner TG, Nagel G, Hegemann P (2011) Light modulation of cellular cAMP by a small bacterial photoactivated adenylyl cyclase, bPAC, of the soil bacterium Beggiatoa. J Biol Chem 286:1181–1188.

Stillman M, Malik B (2008) Chemotherapy-induced peripheral neuropathy. Curr Pain Headache Rep 12:165–174.

Stone MC, Nguyen MM, Tao J, Allender DL, Rolls MM (2010) Global up-regulation of microtubule dynamics and polarity reversal during regeneration of an axon from a dendrite. Mol Biol Cell 21:767–777.

Strahler AN (1952) Hypsometric (area-altitude) analysis of erosional topography. Bull Geol Soc Am 63:1117–1142.

Südhof TC (2001) α-Latrotoxin and Its Receptors: Neurexins and CIRL/Latrophilins. Annu Rev Neurosci 24:933–962.

Tracey WD, Wilson RI, Laurent G, Benzer S (2003) painless, a *Drosophila* gene essential for nociception. Cell 113:261–273.

Tsakiri EN, Terpos E, Papanagnou ED, Kastritis E, Brieudes V, Halabalaki M, Bagratuni T, Florea BI, Overkleeft HS, Scorrano L, Skaltsounis AL, Dimopoulos MA, Trougakos IP (2017) Milder degenerative effects of Carfilzomib vs. Bortezomib in the *Drosophila* model: A link to clinical adverse events. Sci Rep 7:1–12.

Tsubouchi A, Caldwell JC, Tracey WD (2012) Dendritic filopodia, ripped pocket, NOMPC, and NMDARs contribute to the sense of touch in *Drosophila* larvae. Curr Biol 22:2124–2134.

Veldhuis NA, Poole DP, Grace M, McIntyre P, Bunnett NW (2014) The G Protein-Coupled Receptor-Transient Receptor Potential Channel Axis: Molecular Insights for Targeting Disorders of Sensation and Inflammation. Pharmacol Rev 67:36–73.

Voolstra O, Huber A (2014) Post-Translational Modifications of TRP Channels. Cells 3:258–287.

Walcott KCE, Mauthner SE, Tsubouchi A, Robertson J, Tracey WD (2018) The *Drosophila* Small Conductance Calcium-Activated Potassium Channel Negatively Regulates Nociception. Cell Rep 24:3125-3132.e3.

Wässle H, Peichl L, Boycott BB (1981) Dendritic territories of cat retinal ganglion cells. Nature 292:344–345.

Xiang Y, Yuan Q, Vogt N, Looger LL, Jan LY, Jan YN (2010) Light-avoidance-mediating photoreceptors tile the *Drosophila* larval body wall. Nature 468:921–926.

Xiong X, Hao Y, Sun K, Li J, Li X, Mishra B, Soppina P, Wu C, Hume RI, Collins CA (2012) The Highwire Ubiquitin Ligase Promotes Axonal Degeneration by Tuning Levels of Nmnat Protein. PLoS Biol 10:1–18.

Xiong X, Wang X, Ewanek R, Bhat P, DiAntonio A, Collins CA (2010) Protein turnover of the Wallenda/DLK kinase regulates a retrograde response to axonal injury. J Cell Biol 191:211–223.

Yan Z, Zhang W, He Y, Gorczyca D, Xiang Y, Cheng LE, Meltzer S, Jan LY, Jan YN (2013) *Drosophila* NOMPC is a mechanotransduction channel subunit for gentle-touch sensation. Nature 493:221–225.

Yekkirala AS (2013) Two to tango: GPCR oligomers and GPCR-TRP channel interactions in nociception. Life Sci 92:438–445.

Yoshino J, Morikawa RK, Hasegawa E, Emoto K (2017) Neural Circuitry that Evokes Escape Behavior upon Activation of Nociceptive Sensory Neurons in *Drosophila* Larvae. Curr Biol 27:2499-2504.e3.

Zelle KM, Lu B, Pyfrom SC, Ben-Shahar Y (2013) The Genetic Architecture of Degenerin/Epithelial Sodium Channels in *Drosophila*. G3 Genes|Genomes|Genetics 3:441–450.

Zhang M, Wang Y, Geng J, Zhou S, Xiao B (2019) Mechanically Activated Piezo Channels Mediate Touch and Suppress Acute Mechanical Pain Response in Mice. Cell Rep 26:1419-1431.e4.

Zhong L, Hwang RY, Tracey WD (2010) Pickpocket Is a DEG/ENaC Protein Required for Mechanical Nociception in *Drosophila* Larvae. Curr Biol 20:429–434.

9 Appendix

9.1 Figures and tables

9.2 Abbreviations

°	degree angle
°C	degree Celsius
7TM	seven transmembrane domain
ADHD	attention deficit hyper-activity disorder
AEL	after egg laying
aGPCR	adhesion-type G protein-coupled receptors
bPAC	bacterial photoactivatable adenylate cyclase
C1da	dorsal arborization neurons class I
C2da	dorsal arborization neurons class II
C3da	dorsal arborization neurons class III
C4da	dorsal arborization neurons class IV
CaM	calmodulin
cAMP	cyclic adenosine monophosphate
ChO	chordotonal organ
CIRL	Ca_{2+} independent receptor of latrotoxin
CNS	central nervous system
cpGFP	circularly permuted green fluorescent protein
CTF	C-terminal fragment
da	dorsal arborization
DEG	degenerin
DMSO	dimethyl sulfoxide
DNA	deoxyribonucleic acid
DRG	dorsal root ganglion
ENaC	epithelial Na_+ channel

g	gramm
GAIN	GPCR autoproteolysis inducing domain
GFP	green fluorescent protein
GPS	proteolysis site
h	hours
HL-3	hemolymph-like saline
HRM	hormone binding domain
Hz	Herz
iav	inactive
IPN	induced peripheral neuropathy
kg	kilogram
KO	knockout
l	liter
LPHN	Latrophilin
ml	milliliter
mm	millimeter
mm$_2$	square millimeter
n.s.	not significant
nan	nanchung
nls	nuclear localization sequence
Nm	newton meter
NMJ	neuromuscular junction
NMNAT	nicotinamide mononucleotide adenylyltransferase
NompC	no mechanoreceptor potential C
NTF	N-terminal fragment
Ø	diameter

OE	overexpression
OLF	olfactomedin-like domain
PDE	phosphodiesterase
PFA	paraformaldehyde
PNS	peripheral nervous system
ppk	pickpocket
RBL	rhamnose binding lectin-like domain
RFP	red fluorescent protein
RNA	ribonucleic acid
RNAi	RNA-interference
SEM	standard error of mean
td	tandem dimer
TEN	Teneurin
TRP	transient receptor channel
TRPA	transient receptor channel ankyrin
TRPC	transient receptor channel canonical
TRPM	transient receptor channel melastatin
TRPML	transient receptor channel mucolipin
TRPN	transient receptor channel NOMPC like
TRPP	transient receptor channel polycsctin
TRPV	transient receptor channel vanilloid
UAS	upstream activating sequence
V/D/A/P	ventral / dorsal / anterior / posterior
WT	wildtype
μm	micrometer
μW	micro Watt

9.3 Curriculum vitae

9.4 Affidavit

Affidavit

I hereby confirm that my thesis entitled "**Function of the *Drosophila* adhesion-GPCR Latrophilin/CIRL in nociception and neuropathy"** the result of my own work. I did not receive any help or support from commercial consultants. All sources and / or materials applied are listed and specified in the thesis.

Furthermore, I confirm that this thesis has not been submitted as part of another examination process neither in identical or similar form.

Würzburg,

Place, Date   Signature

Eidesstattliche Erklärung

Hiermit erkläre ich an Eides statt, die Dissertation „**Funktionelle Rolle des *Drosophila* aGPCR Latrophilin/CIRL in Nozizeption und Neuropathie"** eigenständig, d.h. insbesondere selbstständig und ohne Hilfe eines kommerziellen Promotionsberaters, angefertigt und keine anderen als die von mir angegebenen Quellen und Hilfsmittel verwendet zu haben.

Ich erkläre außerdem, dass die Dissertation weder in gleicher noch in ähnlicher Form bereits in einem anderen Prüfungsverfahren vorgelegen hat.

Würzburg,

Ort, Datum   Unterschrift